pubs.acs.org/Biomac

Article

Contributions of Crystalline and Noncrystalline Cellulose Can Occur in the Same Spectral Regions: Evidence Based on Raman and IR and Its Implication for Crystallinity Measurements

Umesh P. Agarwal,* Sally A. Ralph, Carlos Baez, and Richard S. Reiner

Cite This: *Biomacromolecules* 2021, 22, 1357−1373

Read Online

ACCESS | Metrics & More | Article Recommendations | Supporting Information

ABSTRACT: Aggregated states of celluloses remain poorly understood, and therefore, the topic requires careful investigation. In this study, Raman, IR, and X-ray diffraction (XRDs) were used to study cotton microcrystalline cellulose (MCC) and MCC that has been ball-milled to various degrees. Raman and IR spectroscopy methods indicated that when these ball-milled samples were wet with water, most underwent conformational changes at the molecular level. Although formation of cellulose II was observed in longer duration ball-milled samples, the changes primarily gave rise to increased contributions in spectral and diffraction regions typically associated with the contributions of crystalline cellulose I. Moreover, when the wet samples were air-dried at 25 °C, the newly formed cellulose I-like structures partly reverted to the previous form present in the initial dry state. These findings explained for the previously reported XRD and NMR observations, where the addition of water resulted in increased crystallinities of cellulose samples. The implications of these findings to cellulose crystallinity measurements and other situations are discussed.

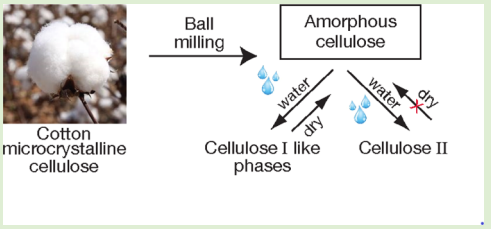

INTRODUCTION

In nature, cellulose is produced by a large number of organisms ranging from bacteria to plants. In its native state, depending upon the function of the organisms, cellulose exists in a variety of self-organized supramolecular structures which differ mainly with respect to intra- and inter-molecular noncovalent interactions.[1,2] Although two main phases of such structures, namely, crystalline and amorphous, are widely recognized, defining the intermediate states has proven to be a complicated problem and is quite challenging. In the absence of this, terms such as paracrystalline, non-crystalline, semicrystalline, ordered, disordered, organized, and disorganized are used.[3−7] However, strictly speaking, even to be called amorphous, the phase has to be uniformly disordered, which may not be the case in reality. Knowledge of the supramolecular structure of cellulose is essential in a great number of areas, for example, plant science, biofuels, pulp and paper, and cellulose nanomaterials.

Moreover, in cellulose and related fields, many unresolved questions still need to be clarified by further research. Questions such as, why the crystallinity (CrI) of wood-pulp derived cellulose nanocrystals (CNCs) is not significantly higher than that of the pulp[8] and is the often-invoked phenomenon of cocrystallization real arise.[9−13] Lastly, are the moisture-induced changes in the X-ray diffractions (XRDs) of woods and celluloses due to changes in the unit cell dimensions[7,14−16] or, as proposed by Agarwal et al.,[16] due to the reorganization of cellulose? Furthermore, considering the structure−property−function relationships, the topic under study is a critical problem to solve so that the structures can be defined more precisely. Therefore, it is imperative that the terms describing the aggregated states of cellulose be better defined to obtain a comprehensive molecular-level understanding of the many phases of cellulose. One area of impact where such a development is going to be important is estimation of the cellulose CrI because various aggregated states of cellulose are seen differently by the methods used to estimate it.[17] In this context, recent findings have suggested the existence of spatially ordered cellulose (e.g., a mono layer thick lamella of cellulose chains) which contributed in the same regions where contributions of crystalline domains are detected.[18−20] Therefore, although not crystalline, such entities are likely to influence the estimates of CrI by most methods (e.g., NMR, XRD, and Raman spectroscopy). The ultrathin microfibrils (cellulose microfibrils are ∼3 nm thick) are fractions, which are only molecularly thick (0.5 nm) and contained only a single layer of cellulose chains, are assemblies of cellulose which are non-crystalline. On the other hand, in the authors' work,[5,6,21] a similar limitation of the 380-Raman, a method for estimating CrI, was encountered when it was used to calculate the CrI of native wood celluloses. For instance, the

Received: September 25, 2020
Revised: March 15, 2021
Published: March 26, 2021

https://doi.org/10.1021/acs.biomac.0c01389
Biomacromolecules 2021, 22, 1357−1373

method produced CrI values of 49.9 and 57.4% for aspen and red pine wood celluloses, respectively, although the later work established that wood cellulose is non-crystalline.[5,6] This further supported the argument that simply ordered, and not crystalline cellulose, may make contributions in the spectral/diffraction regions that are typically associated with crystalline cellulose. Moreover, in XRD, the diffraction patterns of wood and other low-CrI celluloses showed high sensitivity to moisture—depending upon the samples, the crystallinity increased by as much as 40%,[16] thereby supporting the existence of spatially organized but non-crystalline cellulose. Another example of higher cellulose XRD CrI in the presence of water was reported for several wood species.[7] Likewise, by ^{13}C NMR, increases of CrIs were observed in wet cellulose materials,[22,23] once again providing evidence in support of cellulose reorganization in the presence of water and thereby causing an increase in the CrIs. In the work that investigated cotton fibers at various days post-anthesis (DPAs),[24] at 17 DPA, non-crystalline cellulose had contributions at 2θ positions in XRD where the (200) plane of crystalline cellulose contributed. However, no peak at 380 cm^{-1} was detected in Raman spectroscopy indicating that the cellulose was indeed non-crystalline in nature.[25]

Therefore, given the strong indications from the published studies that organized cellulose structures contribute in the same spectral/diffraction regions as crystalline cellulose, a study was undertaken to find out if indeed it is so. For this purpose, cotton microcrystalline cellulose (MCC) (crystals that are visible only under a microscope) and its ball-milled-to-various-degrees samples were selected for investigation. The milled samples were chosen as representative of lower crystallinity celluloses. Although MCC is a highly crystalline material (Segal CrI 89.4%), CrIs of the milled samples depend upon the duration of ball-milling (see below).[25] All the samples were derived from the same source and were made up almost entirely of cellulose, therefore only changes caused by ball-milling, such as those in crystallinity and the structures, would be relevant in this study. Water was utilized as a means for altering the supramolecular structures of the samples. Effects of wetting and drying-post-wetting were investigated using Raman, IR, and XRD. The first two methods being molecular spectroscopy techniques are well suited to detect changes in cellulose at the molecular level. Raman spectroscopy has the added advantage that the water contributions are minimally detected and the fact that the authors have advanced Raman methods to characterize the supramolecular structure of cellulose.[5,6,23,25]

MATERIALS AND METHODS

Chemicals. Unless stated otherwise, all chemicals and reagents, including D_2O (99.9% deuterated), were purchased from Sigma-Aldrich (St. Louis, MO).

Celluloses. Whatman CC31 powder (cotton MCC) was purchased from Whatman International Ltd. (Maidstone, UK). Lower crystallinity and amorphous cellulose samples were generated by milling, for various durations, cotton MCC in a vibratory mill using steel balls. As reported previously,[25] the milling was conducted in a cold room (5 °C) for a prescribed time. The ball-milling times were 2.5, 5, 10, 15, 30, 45, 60, 90, and 120 min. The milling reduced the crystallinity of cotton MCC and based on previously reported Raman spectroscopy and XRD results, the 120 min sample was interpreted as completely amorphous cellulose.[5,25]

Bleached Pulp. Never dried softwood bleached kraft pulp was supplied by NewPage Miamisburg, Ohio. The pulp was thoroughly washed with water prior to analysis. A portion of this pulp was dried in an oven at 105 °C for 18 h. A part of the oven-dried pulp was wet again by immersing a small amount in RO water. The pulp samples were analyzed using Raman spectroscopy.

Scanning Electron Microscopy Imaging. Control and the ball-milled cotton MCC samples were examined and photographed with a Zeiss EVO 40 SEM (Carl Zeiss SMT Inc., Thornwood, NY). The particles were dispersed in water on polished aluminum mounts and air dried. The samples were sputter-coated with gold using a Denton Desk-1 sputter coater (Cherry Hill, NJ) to provide sufficient conductivity.

Recording Raman Spectra and Band Intensity Calculations. Control and ball-milled cotton MCC samples were analyzed, in triplicate, with a Bruker MultiRam spectrometer (Bruker Instruments Inc., Billerica, Massachusetts). The Raman system is equipped with a 1064 nm 1000 mW continuous wave diode pumped Nd:YAG laser. Approximately 20 mg of dry powder of each sample was put in a shortened NMR tube, and its Raman spectrum was recorded using a 600 mW laser power. Depending upon the S/N desired, 1024−2048 scans were co-added. Subsequently, the sample was wet by adding a small amount (0.2 mL) of water in the NMR tube, and the contents mixed well with a thin metal rod. Subsequently, the sample tube was centrifuged so that the sample was settled at the bottom of the tube. The wet and well-mixed sample was analyzed by Raman spectroscopy. Similarly, for dry-after-wet sample analysis, another aliquot of each sample was wet in water in a open Petri dish and then allowed to stand for drying at 25 °C for 48 h (until completely dry). Once dried, Raman spectra were obtained under identical experimental conditions. Additionally, spectra from the initial dry state of the samples were obtained in the pellet form. For this, approximately 0.10 g of each sample was pressed into a pellet with the help of a hydraulic press. To make a pellet, ~276×10^6 dyn/cm^2 of compressive pressure was applied.

The laser power used for sample excitation was 600 mW, and 1024 scans were accumulated. Bruker OPUS 7.2 software was used to determine peak positions and process the spectral data. The processing of spectra involved background removal, normalization at 1096 cm^{-1}, and various mathematical operations. Background correction was performed using the "rubber band option" in OPUS using 64 baseline points. Peak heights in the normalized spectra were calculated for 1096, 1380, and 1480 cm^{-1} bands by drawing a horizontal baseline under each of the bands. The line was drawn, respectively, from 944, 1445, and 1500 cm^{-1}. On the other hand, for 380 and 577 cm^{-1} peaks, a sloping baseline method of integration was used. For this, respectively, sloping lines between 370 and 395 and 571 and 588 cm^{-1} were drawn. Moreover, for the band intensity of the 577 cm^{-1} band, the contribution at this position from the 562 cm^{-1} band in the control sample was deducted from all of the measured 577 cm^{-1} band intensities. Intensity measurements from triplicate Raman analyses indicated in all cases that the SD was <3%. For plotting purposes, the spectra were converted to ASCII format which then allowed the spectral data to be exported to Excel.

Because a Raman-based cellulose CrI method, 380-Raman,[25] is linearly correlated to the ratio I_{380}/I_{1096}, in this work, as a representative of CrI, only the intensity ratio was calculated.

For calculating accessibility to water (A), as described previously,[5,26] first, a Raman spectrum was obtained from ca. 20 mg of a sample in H_2O. Subsequently, another 20 mg of aliquot of the same sample is analyzed in D_2O after the sample has undergone a complete OH-to-OD exchange. The latter can be achieved by removing excess H_2O (from never-dried materials) and putting the sample in D_2O. This was followed by centrifugation (4000 × g) in a centrifugal filter (Amicon, Ultra-4, Ultracel-30K, Merck Millipore Ltd.) until excess D_2O is removed. Thereafter, this process was repeated until the sample's 1380 cm^{-1} band intensity did not increase anymore (usually 3 or 4 times), implying that most replaceable OHs are exchanged with ODs. From 1096 cm^{-1}, normalized spectra 1380 cm^{-1} intensities were measured from spectra obtained in H_2O and in D_2O (OH-to-OD exchanged), and eq 1 below was used to calculate accessibility.

https://doi.org/10.1021/acs.biomac.0c01389
Biomacromolecules 2021, 22, 1357−1373

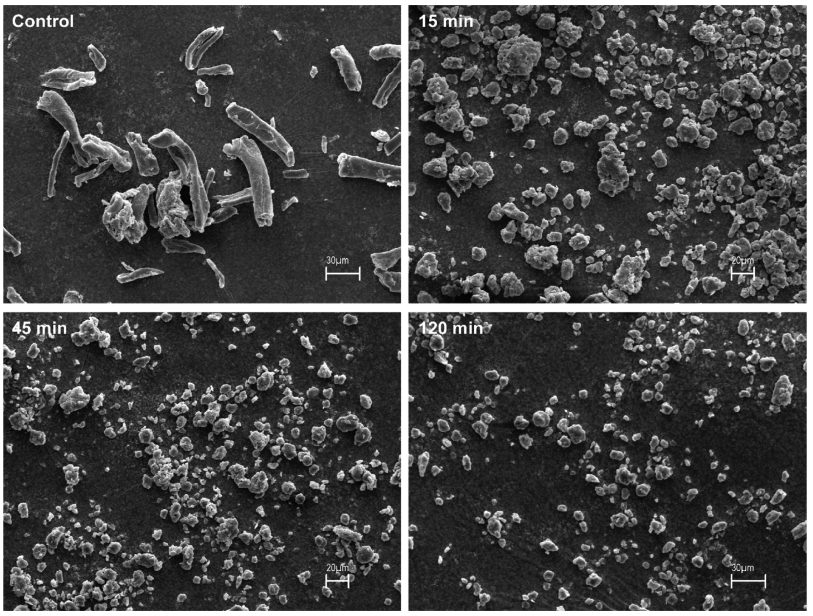

Figure 1. SEMs of MCC samples; control, 15, 45, and 120 min ball-milled.

$$\text{Accessibility (Raman)} = \Delta I_{1380(\text{sample})} \times 100/\Delta I_{1380(\text{amorphous})} \quad (1)$$

where ΔI_{1380} (sample) and ΔI_{1380} (amorphous) are, respectively, 1380 cm^{-1} band intensity increases for sample and amorphous cellulose.[5,24]

Estimation of Cellulose I and Cellulose II Amounts from Raman Spectra. The amounts of cellulose I plus cellulose I-like and cellulose II present in samples other than the dry-state control sample were estimated based on the relative peak heights of the bands present, respectively, at 380 and 577 cm^{-1}. In the case of the dry-state control sample, the amount of cellulose I, 89.7%, was taken from the XRD measurement (Figure 2a). In the case of the dry-state control sample, the Raman intensity ratio I_{380}/I_{1096} was assigned this value, and for all other samples, the cellulose I amount, which also included the cellulose I-like phase, was calculated from eq 2 below.

$$\%\ \text{cellulose I} = \left[\frac{\left(\frac{I_{380}}{I_{1096}}\right)\text{sample}}{\left(\frac{I_{380}}{I_{1096}}\right)\text{dry-state control}}\right] \times 89.7 \quad (2)$$

Similarly, cellulose II amount was estimated based on the peak intensity of 577 cm^{-1} band (eq 3). Previously, it has been reported that in mixed cellulose I and cellulose II polymorph samples, Raman spectroscopy is capable of successfully estimating the amount of cellulose II present.[27] In the following equation, 100% cellulose II was taken to be a sample of fully mercerized Avicel PH-101, a Raman spectrum of which is shown in Figure S1.

$$\%\ \text{cellulose II} = \left[\frac{\left(\frac{I_{577}}{I_{1096}}\right)\text{sample}}{\left(\frac{I_{577}}{I_{1096}}\right)\text{cellulose II}}\right] \times 100 \quad (3)$$

Fourier-Transform Infrared Spectroscopy. Attenuated total reflection (ATR) Fourier-transform infrared (FT-IR) spectra of dry, wet, and dry-after-wet cotton MCC samples were obtained on a Spectrum Two, PerkinElmer, Waltham, MA system that was equipped with a universal ATR probe. An ATR spectrum of a dry sample was obtained first. A few drops of water were then added, and the sample was mixed thoroughly and sampled again. For recording ATR spectra of dry-after-wet samples, another aliquot of each of the samples was wet in water and then dried at 25 °C in air until completely dry (usually for 48 h). An IR spectrum was obtained using the same instrument settings as used above for the dry and wet samples. The spectra were obtained in the range of 450−4000 cm^{-1} with a resolution of 4 cm^{-1}. IR spectra were processed using OPUS 7.2, and the ASCII files were imported in Excel for plotting purposes. The IR spectra were not background corrected but normalized at 1020 cm^{-1}. From the normalized spectra, band intensities for 1020, 1315, and 1430 cm^{-1} peaks were calculated using the following methods. For the 1020 and 1315 cm^{-1} bands, peak heights were measured by drawing horizontal baselines, respectively, under the bands at 920 and 1295 cm^{-1}. On the other hand, for 1430 cm^{-1} peak, a sloping baseline method was used due to substantial overlaps from the neighboring bands. For this, a sloping line was drawn between 1480 and 1410 cm^{-1}.

XRD and Segal-WAXS CrI Calculation. Wide-angle XRD profiles were recorded in the reflection mode on a Bruker D8 Discover diffractometer with a monochromatic Cu Kα (λ = 1.5418 Å) point source and a VÅNTEC-500 detector at the Materials Research Science and Engineering Center, University of Wisconsin, Madison. The X-ray diffractometer beam aperture of 0.5 mm was used. In all cases, first, diffractograms were obtained on the dry samples (9 mm diameter sample pellet form). Subsequently, 5 μL of water was added to the center of the pellet (100 mg) surface using a syringe. Once the water disappeared from the surface and was absorbed by the pellet, a diffractogram was obtained. Then, the pellet was turned over, and the other side was analyzed. Additional water was not applied to the other side. Lastly, for the dry-after-wet XRD analysis, pellets (100 mg each) were made from the same dry-after-wet materials that were used in Raman spectroscopy. Once again, both sides of the pellet were sampled. Average values of the CrIs are reported. Segal-WAXS CrI was calculated by measuring the (200) peak intensity, I_{200}, and subtracting the amorphous contribution, I_{am}, at approximately 2θ = 18° (eq 4).[28]

$$\text{CrI} = 100 \times (I_{200} - I_{am})/I_{200} \quad (4)$$

In the diffractograms of some samples, especially those ball-milled for a longer duration, no minimum/inflection at ~18° 2θ was detected, but Segal CrI was still calculated by measuring amorphous contribution at this 2θ position.

RESULTS AND DISCUSSION

Overview on Ball-Milled MCC. Figure 1 shows scanning electron microscopy (SEM) of the control and selected balled-milled samples (15, 45, and 120 min). The SEMs indicated that upon 15 min of ball-milling, most of the MCC fibers were

https://doi.org/10.1021/acs.biomac.0c01389
Biomacromolecules 2021, 22, 1357−1373

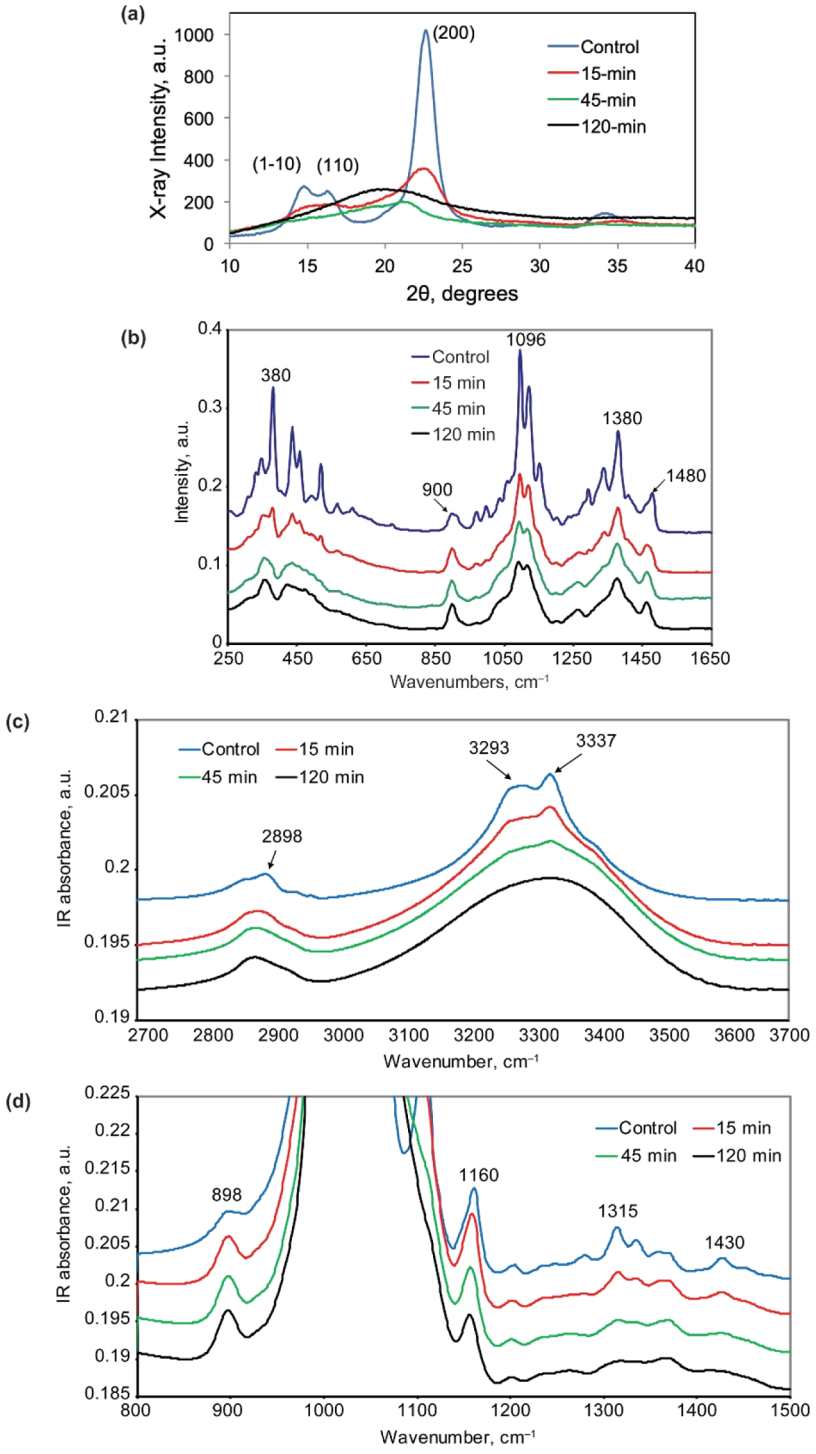

Figure 2. X-ray diffractograms and Raman and IR spectra of control and selected ball-milled samples in the initial dry state: (a) XRDs, (b) Raman spectra, and (c,d) IR spectra. In plots (b–d), spectra were offset on the intensity scale for display purposes. Segal CrIs for (a) samples—control, 15, 45, and 120 min BM samples were, respectively, 89.7, 67.8, 45.1, and 23.7%.

reduced in size (Figure 1, 15 min). Additional milling continued this morphological change of shape and size, and the control sample which had fiber-like appearance (Figure 1, control) transformed to numerous sphere-like particles much reduced in size (Figure 1). After 120 min of ball-milling, there was no residual fiber-like material left (Figure 1, 120 min).

XRDs of control and selected ball-milled samples in the dry state are shown in Figure 2a. Segal CrIs of the samples are also noted in the legend of this figure. Based on the diffractograms of the four samples and their CrIs, it is clear that the control sample rapidly decrystallized upon ball-milling. Within 45 min of milling, the CrI drops by >50%. After that, upon continued milling, crystallinity dropped only slowly. Because the Segal method becomes less reliable for the longer duration ball-milled samples due to both absence of a minimum at ∼18° 2θ and increased contributions from amorphous (XRD peak occurs at 20.9°) and disordered states at ∼22.6° 2θ, the CrI data for 45 and 120 min samples are less reliable. In the

https://doi.org/10.1021/acs.biomac.0c01389
Biomacromolecules 2021, 22, 1357−1373

diffractograms, the overall peak profiles are determined by heights, widths, and positions of the overlapping peaks (Figure 2a) which, in turn, are contributions of various aggregates/phases of cellulose, likely to be present in the samples. However, the 120 min sample showed a broad smooth curve and thus is considered to be completely amorphous, as reported previously.[5,25]

Raman spectra, in the spectral region 250−1650 cm^{-1}, are shown in Figure 2b. Ball-milling caused intensity to decline in some bands. Of the annotated bands in Figure 2b, intensity declined at 380, 1096, 1380, and 1480 cm^{-1}, but band intensity increased at 900 cm^{-1}. Increased production of disordered/amorphous cellulose was the reason why the band intensities and profiles changed.[25] Whereas cellulose bands 380 and 1096 cm^{-1} are associated with ring stretches and C−C and C−O stretches, respectively, the bands at 1380 and 1480 cm^{-1} belonged to Raman spectroscopy modes of the exocyclic CH_2 group. The vibrational mode at 900 cm^{-1}, where intensity increased upon ball-milling, has been associated with conformational disorder (anomeric vibration β-O-4) in cellulose and is found to be relatively weak in highly crystalline celluloses (e.g., tunicin and algal celluloses). In the past, to estimate cellulose CrI, a Raman method—380-Raman, was developed. The method is based on the band intensity ratio I_{380}/I_{1096}. As reported previously, the 380-Raman method also showed a reduction of cellulose CrI in the ball-milled samples.[25]

IR spectra of the four samples are shown in O−H stretch (3000−3700 cm^{-1}) and finger-print (800−1500 cm^{-1}) regions (Figure 2c,d, respectively). In the O−H stretch region, the band at 3337 cm^{-1} (3342 cm^{-1} in Raman, not shown) due to intramolecular H-bonding (O3−H···O5)[29−32] declined slowly upon ball-milling and disappeared totally in the case of 120 min milled sample (Figure 2c). This disappearance indicated that the original cellulose chain conformation present in the control sample, a highly crystalline material, was completely altered, and therefore, the 120 min milled amorphous sample had its own cellulose conformation. The IR spectra of intermediate samples (15 and 45 min milled samples) showed lower intensity of this band, which was indicative of the increased formation of amorphous cellulose upon ball-milling. Moreover, in the 800−1500 cm^{-1} region (Figure 2d), as was the case in Raman spectroscopy (Figure 2b), several IR bands showed changes in their intensities and profiles. The bands at 898, 1160, 1315, and 1430 cm^{-1} are of interest (see below) and are annotated in Figure 2d. Upon ball-milling, band intensity increased at 898 cm^{-1}, which was also the case in Raman spectroscopy. On the other hand, the intensity declined for bands at 1160 (C−O−C antisymmetric stretching), 1315 (CH_2 wagging), and 1430 (CH_2 bending) cm^{-1}. It is important to note that band intensity ratios I_{1430}/I_{898}, I_{1280}/I_{1200}, and I_{1372}/I_{2900} have been used for estimation of cellulose CrI in IR.[33−35] In the work described here, the intensity changes observed at 1430 cm^{-1} would therefore be of particular interest. It has been reported that the changes observed in IR spectra due to ball-milling are caused by the mechanical treatment itself and not by particle size reduction or oxidation processes.[30]

Raman Spectroscopy. *Effect of Wetting on Raman Spectra.* For selected samples (control, 15, 45, and 120 min ball-milled), Raman spectra of initial dry samples are compared with those obtained after wetting and drying-after-wetting (Figure 3). The spectra are plotted after they were normalized

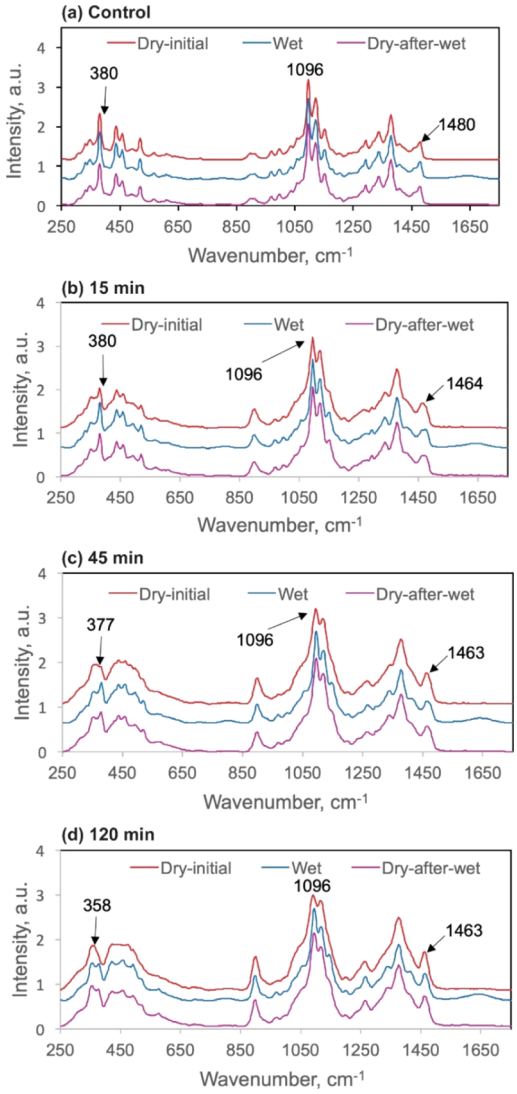

Figure 3. Raman spectra of selected ball-milled samples in initial dry, wet, and dry-after-wet states; (a) control, (b) 15 min ball-milled, (c) 45 min ball-milled, and (d) 120 min ball-milled. In a−d, spectra were offset on the intensity scale for display purposes. The annotated band positions are for the initial dry sample.

at 1096 cm^{-1}. Although many band intensities were affected in the Raman spectra as a result of wetting and drying-after-wetting (Figure 3), only the ratios I_{380}/I_{1096} and I_{1480}/I_{1096} are reported (Table S1). These band ratios were chosen for analysis because they have been previously shown to be associated with cellulose crystallinity.[21,25,36] The percent changes in these two ratios for "wet versus dry" and "dry-after-wet versus wet" are listed in Table 1, and how the I_{380}/I_{1096} ratio varied with the duration of the ball milling in all three states is plotted in Figure 4. For I_{380}/I_{1096}, the % change was calculated using eqs 5 and 6 below. Similarly, for the ratio I_{1480}/I_{1096}, same equations were used and I_{380} was substituted by I_{1480}. Furthermore, upon wetting, most bands were better resolved (e.g., 950−1150 cm^{-1} region; Figure 3), indicating that compared to the dry state, the cellulose wet state had higher order and better organization. For instance, this can be clearly noted in the case of the 45 min ball-milled sample (Figure 3c). Compared to the initial dry-state spectrum, the

https://doi.org/10.1021/acs.biomac.0c01389
Biomacromolecules 2021, 22, 1357−1373

Table 1. % Changes in Raman Band Intensity Ratios[a]

	wet vs dry		dry-after-wet vs wet		initial dry vs dry-after-wet	
samples	(I_{380}/I_{1096})	(I_{1480}/I_{1096})	(I_{380}/I_{1096})	(I_{1480}/I_{1096})	(I_{380}/I_{1096})	(I_{1480}/I_{1096})
control	2.89	−2.00	−18.01	3.13	18.54	−1.06
2.5 min	18.29	−7.39	−23.33	6.98	10.27	0.94
5 min	53.76	−9.77	−25.99	7.70	−12.12	2.90
10 min	66.91	−14.33	−15.95	6.45	−28.72	9.66
15 min	59.96	9.37	−12.66	11.70	−28.42	−18.15
30 min	441.13	−24.89	−41.36	12.66	−68.48	18.18
45 min	DZ[b]	−23.68	−21.74	17.39	−100.0	11.62
60 min	DZ	−26.80	−28.72	14.04	−100.0	19.79
90 min	DZ	−27.57	−33.30	16.26	−100.0	18.75
120 min	DZ	−29.49	−25.29	14.56	−100.0	23.79

[a]Negative values mean decline in intensity. [b]DZ because of divide-by-zero could not be calculated.

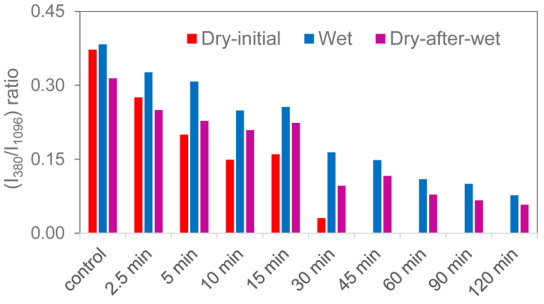

Figure 4. Raman band intensity ratio I_{380}/I_{1096} in the spectra of control and ball-milled samples in dry (initial), wet, and dry-after-wet states.

entire fingerprint region of the wet-sample spectrum was better resolved.

$$\text{Change}_{\text{wet vs dry}} = [(I_{380}/I_{1096})_{\text{wet}} - (I_{380}/I_{1096})_{\text{dry}}] \times 100/(I_{380}/I_{1096})_{\text{dry}} \quad (5)$$

$$\text{Change}_{\text{dry-after-wet vs wet}} = [(I_{380}/I_{1096})_{\text{dry-after-wet}} - (I_{380}/I_{1096})_{\text{wet}}] \times 100/(I_{380}/I_{1096})_{\text{wet}} \quad (6)$$

$$\text{Change}_{\text{dry vs dry-after-wet}} = [(I_{380}/I_{1096})_{\text{dry}} - (I_{380}/I_{1096})_{\text{dry-after-wet}}] \times 100/(I_{380}/I_{1096})_{\text{dry-after-wet}} \quad (7)$$

As mentioned above, because 380 and 1480 cm^{-1} bands have been used to estimate cellulose crystallinity,[21,25,36] they were of particular interest. Upon wetting, in the spectra of the ball-milled samples, band ratios I_{380}/I_{1096} and I_{1480}/I_{1096} showed significant intensity changes (Tables S1 and 1). However, in some instances, the changes were in opposite directions. Generally speaking, upon wetting, the intensity increased for the I_{380}/I_{1096} case and declined for the I_{1480}/I_{1096}.

First, considering the wet state intensity changes in Table 1 [I_{380}/I_{1096} and Figure 5 (380 cm^{-1} band)] of the values calculated (by eq 5 above), the highest % increase (441%, Table 1) was observed for the 30 min ball-milled sample.

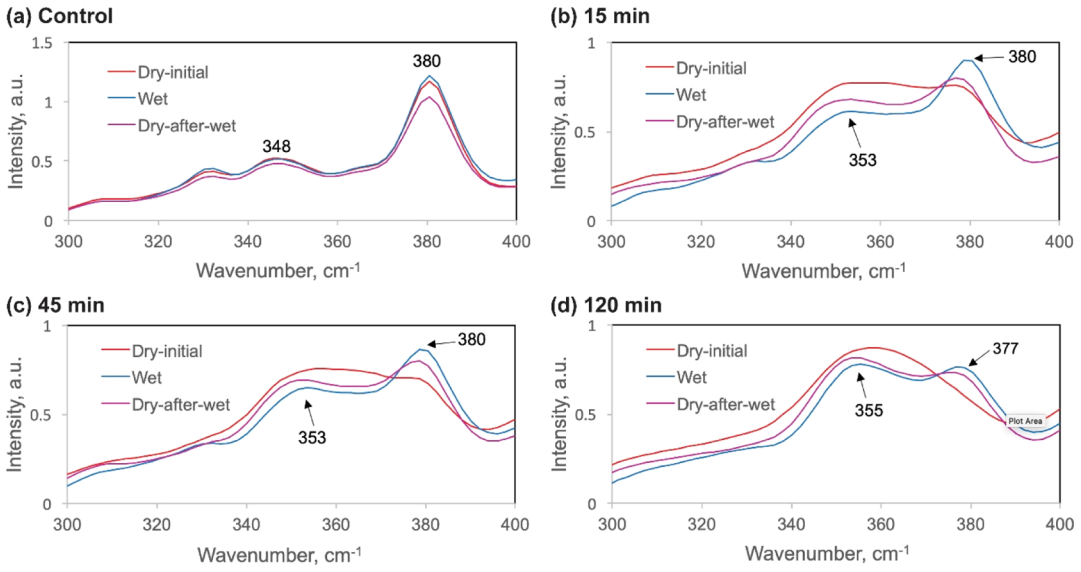

Figure 5. Raman spectra of selected samples in three states of aggregation in the 300−400 cm^{-1} region; (a) control and (b) 15, (c) 45, and (d) 120 min ball-milled samples. The annotated band positions are in the wet-state spectra.

https://doi.org/10.1021/acs.biomac.0c01389
Biomacromolecules 2021, 22, 1357−1373

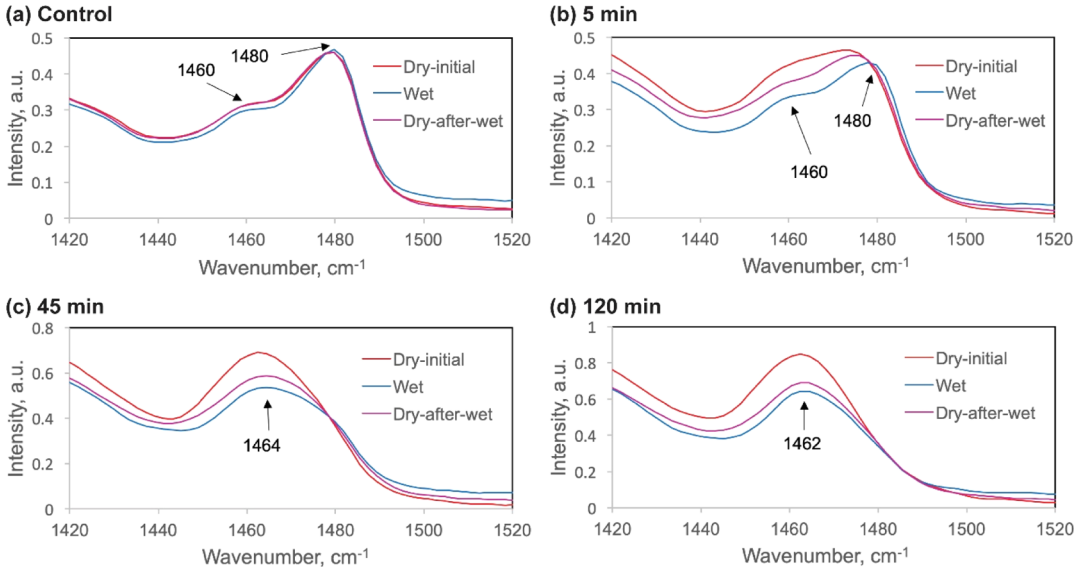

Figure 6. Raman spectra of selected samples in the three states of aggregation in 1420−1620 cm^{-1} region; (a) control and (b) 5, (c) 45, and (d) 120 min ball-milled samples. The annotated band positions are in the wet-state spectra.

However, for samples ball-milled 45 min and longer which lacked the 380 cm^{-1} peak in the dry state, the % increase could not be calculated because of "divide by zero" situation (Table 1). Nevertheless, post wetting, for these samples, water-induced reorganization of cellulose led to appearance of the 380 cm^{-1} peak with considerable intensity (e.g., Figure 5c,d). In addition to changes at ∼ 380 cm^{-1}, the band at 355 cm^{-1} also gained intensity which is a position where cellulose II (Figure S1) is known to contribute (see below, cellulose II formation).[37] Formation of cellulose II from completely amorphous cellulose at 25 °C upon water contact is a well-known phenomenon.[38−40]

Next, we will consider changes in I_{1480}/I_{1096} ratio which declined in most cases upon wetting (Table 1). This decline could be explained by the possibility that while wetting led to increased order between the cellulose chains, the intensity also increased at 1096 cm^{-1} (C−C and C−O stretch mode). Although intensity may have increased in both the bands, the increase at 1096 cm^{-1} may have been higher compared to 1480 cm^{-1} increment, and therefore, the ratio declined compared to its value in the dry state (Table S1). Another complication arises due to the formation of cellulose II, particularly in longer duration ball-milled samples. When cellulose II is formed, it gives rise to a Raman band at 1460 cm^{-1} which is a position 20 cm^{-1} lower compared to where cellulose I-like structures will contribute.[37] The net result being that the overall band profile maximum may be pulled toward the lower frequency region, and hence, increased contribution at 1480 cm^{-1} is not detected. Although, as expected, in the highly crystalline control sample (CrI 89.4%), the band profile of 1480 cm^{-1} feature did not change much upon wetting (Figure 6a), for the short-duration milled samples, wetting produced a better resolved 1480 cm^{-1} band (e.g., 5 min milled sample, Figure 6b). This indicated that in the 5 min milled sample, the number of ordered cellulose chains increased due to wetting. Nevertheless, in some cases (e.g., 2.5, 5, and 10 min ball-milled samples) compared to the dry state, the wet state ratio I_{1480}/I_{1096} was smaller (Table S1) and showed a decline (up to 14%, Table 1). The other complicating factor for the 1480 cm^{-1} peak is that not only it shifts slightly (e.g., Figure 6b) but also overlaps with the neighboring band at ∼1460 cm^{-1} (due to amorphous form and cellulose II, when present; see above), thereby making the intensity measurements at 1480 cm^{-1} somewhat inaccurate. The 1480 and 1460 cm^{-1} bands represent, respectively, the crystalline cellulose I/ordered cellulose and amorphous/disordered states.[5,36,37]

In the wet-state spectra of the short-duration milled samples (i.e., 2.5−15 min ball-milled samples), the reappearance of the peak at 1480 cm^{-1} was seen (e.g., Figure 6b). This result clearly indicated that hydration caused regeneration of cellulose I-like structures. The question still remains, nonetheless, if these water-regenerated forms are indeed crystalline or ordered and non-crystalline phases (more later). In any case, irrespective of the 1096 cm^{-1} intensity issue, the wet-state spectra of longer duration ball-milled samples, no clearly resolved feature at 1480 cm^{-1} was observed (e.g., Figure 6c,d). However, in the absence of clear evidence from the 1480 cm^{-1} region, the 380 cm^{-1} band intensity changes and increased resolutions in the spectra are definite indications of the formation of cellulose I-like structures upon wetting from the amorphous cellulose.

As far as the mechanism of non-crystalline cellulose becoming organized cellulose is concerned, the authors envision the following process. Water is a known swelling agent/plasticizer for cellulose and provides molecular mobility that is sufficient to allow structural transformation. In the amorphous state, upon water association, the conformations of cellulose chains are likely to be modified due to cellulose−water interactions to cellulose I-like and cellulose II conformations as the highly structured water layers around cellulose macromolecules create favorable thermodynamic conditions for such reorganizations. Subsequently, aggregations of the altered conformations take place due to cellulose−cellulose attractive interactions as they become dominant. Moreover, once formed, the new forms are energetically favored and mostly remain irreversible upon drying.

Effect of Drying-after-Wetting on Raman Spectra. For selected samples (control, 15, 45, and 120 min milled samples), the spectra after air-drying at 25 °C from the wet state are shown in Figure 3 along with the spectra of these

https://doi.org/10.1021/acs.biomac.0c01389
Biomacromolecules 2021, 22, 1357−1373

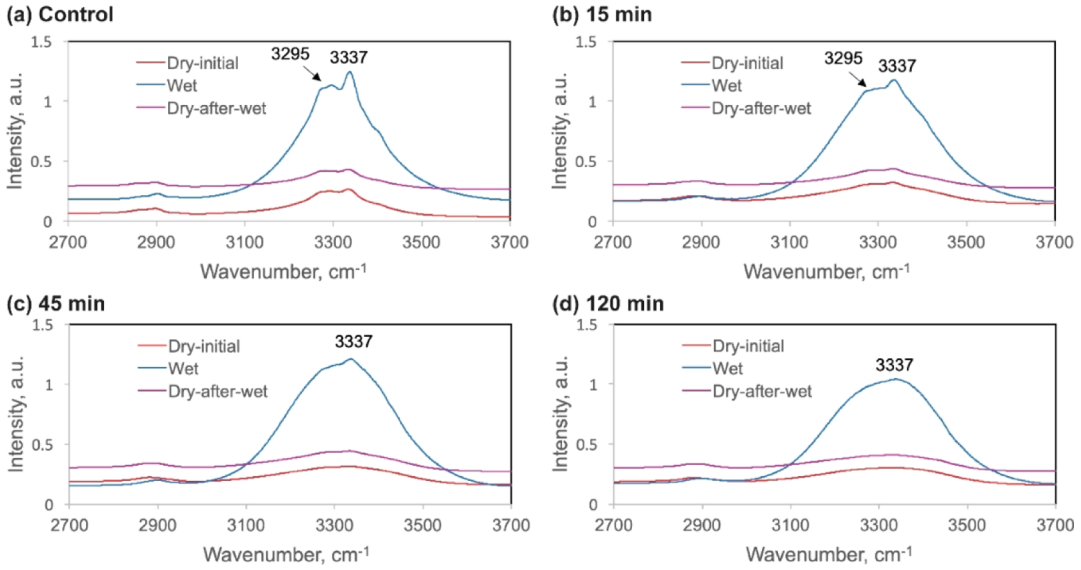

Figure 7. IR spectra of selected samples in the three states of aggregation in the 2700−3700 cm^{-1} region; (a) control and (b) 15, (c) 45, (d) 120 min ball-milled samples. The annotated band positions are in the wet-state spectra.

samples in initial-dry and wet states. The data on band intensity ratios I_{380}/I_{1096} and I_{1480}/I_{1096} are reported in Table S1. The bar plot in Figure 4 shows how the former ratio changes with the duration of milling and with the nature of the state of a sample. Based on eq 6, Table 1 reports the percent change in the two ratios for dry-after-wet compared to the wet state (dry-after-wet vs wet). From this information and reported spectra in Figure 3, the following can be stated. In general, compared to the wet-state spectra, the band resolution declined in the spectra obtained in dry-after-wet states. The spectra in Figure 3 are plotted after normalizing on the 1096 cm^{-1} cellulose band so that the Raman band intensities can be compared directly between the spectra. Compared to the wet state, the ratio I_{380}/I_{1096} in dry-after-wet-state spectra declined in all cases (Table S1, Figure 4). The percent decline, reported in Table 1, was in the range 13−41%, with the lowest and highest decline, respectively, seen for 15 and 30 min milled samples. For the 30 min milled sample, compared to its wet-state conformation, a significant number of chains, 41% (Table 1), became disordered. Although the supramolecular structures in dry-after-wet states of the ball-milled samples became considerably disordered in all cases, wetting-created order was retained to a large extent (Figures 5 and 6 and Table 1). As shown in Figure 6, where Raman band profiles are plotted for 1480 and 1460 cm^{-1} peaks, for 45 and 120 min ball-milled samples, the changes in the profiles were not as straightforward as those in the 380 cm^{-1} band (Figure 5), but the changes supported this observation. It is interesting to note that even in the case of the control sample, the I_{380}/I_{1096} ratio declined by 18% (Table 1) and seems to be due to changes in the intensities of both bands (380 and 1096 cm^{-1}) brought about by how cellulose organizations changed upon wetting and drying-after-wetting. In conclusion, for all samples, such decline meant that the part of the ordered structures that were created by water-induced reorganization became partly disordered. Further considering that such a "loss of order" is not possible with the crystalline cellulose, such structures capable of showing a reversible behavior have to be non-crystalline in nature. Under this characteristic, highly organized non-crystalline assemblies of cellulose would qualify. The rest of the structure that remained irreversible upon drying, post wetting, could be either crystalline, paracrystalline, or coalesced.[3,5,6] In this context, it is noteworthy that recrystallization of mechanically decrystallized cellulose under acid hydrolysis treatment conditions has recently been reported.[41] However, regeneration of crystalline cellulose I has only been reported via precipitation of cellulose from an 85% phosphoric acid solution using glycerol as an antisolvent at 170 °C.[42] Lastly, comparing the initial dry versus dry-after-wet states, it is clear from the data in Table 1, which were calculated using eq 7, that the initial dry states of the samples are quite different from the dry states obtained post wetting. The latter are much more organized because they retain a large part of the wetting-generated organized structures.

IR Spectroscopy. For selected samples (control, 30, 60, and 120 min ball-milled), the effect of wetting on IR spectra of dry and dry-after-wet samples are compared in Figures 7 and 8, respectively, the OH stretch and fingerprint regions. The spectra are plotted after they were normalized at 1020 cm^{-1}. As expected, water intense contributions in the O−H region and at 1640 cm^{-1} in the wet-state spectra were readily detected (Figures 7 and 8). So that a better comparison can be made, for the changes in the OH stretch region, IR spectra for 45- and 120 min samples for initial dry and dry-after-wet states along with the difference spectra are also plotted in Figure S2. From these plots, increased band intensity at 3337 cm^{-1} (for both the samples) and 3440 cm^{-1} (for 120 min sample) can be detected in the dry-after-wet states. Such changes are likely to be due to the conformational changes in cellulose chains due to formation of cellulose I-like and cellulose II upon wetting. Although many band intensities were affected in the IR spectra as a result of not only ball-milling but also upon wetting and drying-after-wetting (e.g., Figure 7b), only band ratios I_{1430}/I_{1020} and I_{1315}/I_{1020} are reported in Table S2. Moreover, how the IR ratios varied with the duration of ball milling and, for each of the ball-milled sample, upon wetting and drying-after-wetting are compared in Figure 9a,b (data in Table S2). The % increases in the band ratios (Table 2) upon wetting compared to the initial dry state were calculated using eq 5 where Raman ratio I_{380}/I_{1096} was replaced either by IR ratio I_{1429}/I_{1020} or IR

https://doi.org/10.1021/acs.biomac.0c01389
Biomacromolecules 2021, 22, 1357−1373

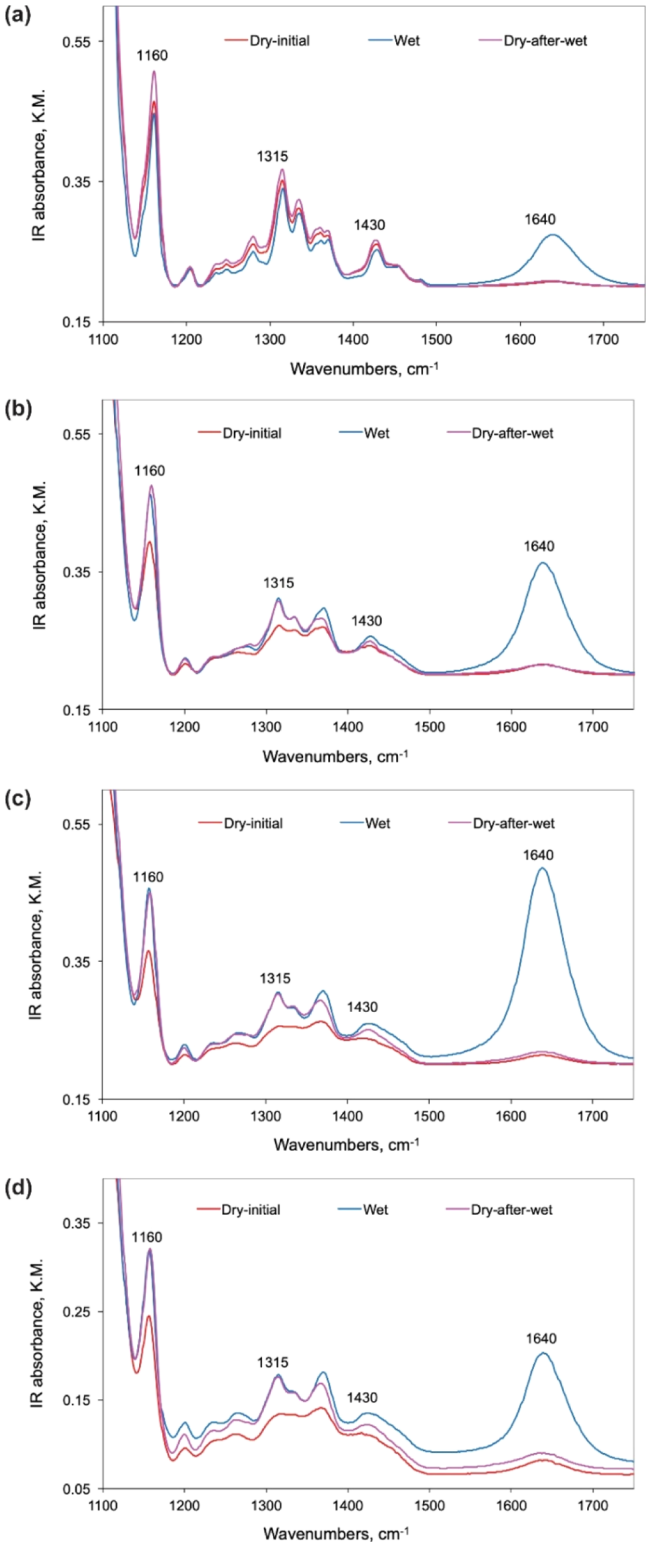

Figure 8. IR spectra of selected samples in the three states of aggregation in the 1100−1700 cm^{-1} region; (a) control and (b) 15, (c) 45, and (d) 120 min ball-milled samples. The annotated band positions are in the wet-state spectra.

ratio I_{1315}/I_{1020}, and these are plotted in Figure 9c,d. The latter figures also show the changes upon drying-after-wetting compared to the wet state (Table 2). Equation 6 was used with the appropriate substitutions of the Raman ratio with the IR ratios, as described above for wet versus dry state comparison. From the data in Table S2 and the plots in Figure 9, it is clear that for most samples, wetting caused large increases in the two band ratios (up to 400 and 165%, respectively, for I_{1430}/I_{1020} and I_{1315}/I_{1020} ratios, Table 2, Figure 9c,d). Additionally, upon wetting, most bands were better resolved (e.g., 1100−1500 cm^{-1} region; Figure 8) indicating that cellulose in the wet state was better organized and had higher order, further supporting the observation already made above by Raman analysis. Analogously, when data from the dry-after-wet state were compared to data in the wet state, the band ratios declined in most cases (decline < 24%, Table 2), although the declines were lower compared to the increases that occurred in going from the initial dry state to wet state (wet vs dry, Table 2). Nonetheless, this decline is very informative because, as in Raman spectroscopy, it indicated that a portion of the wetting-generated structures in cellulose reverted to disordered structures, and therefore, such structures could not be crystalline in nature. Moreover, because these non-crystalline assemblies of cellulose contributed in the same IR regions as crystalline cellulose, the finding is important due to its implication for cellulose crystallinity estimation based on IR.

Lastly, Table 2 data compare the initial dry state with the dry-after-wet state. Once again, the data were calculated as in Raman spectroscopy, using eq 7, with the appropriate substitution by the IR ratios. It is clear that upon drying from the wet state, cellulose chains became partly disorganized in almost every case but, analogous to Raman findings, the samples still retained the majority of the wet-state-generated change. Between the two dry states, the least change was observed for the 2.5 ball-milled sample (because there was not much amorphous cellulose present in the sample), and even the control sample seemed to have undergone some change (Table 2). However, the latter may have to do with how the band integration was performed. Based on the changes to I_{1430}/I_{1020} and I_{1315}/I_{1020} band ratios, the most organizational difference between the two dry states (initial dry vs dry-after-wet) existed in the case of the 60 min milled sample where these ratios were higher, for dry-after-wet states, respectively, by 75 and 58% (Table 2), implying that the state had considerably more order compared to the initial dry state.

X-ray Diffraction. XRDs of selected samples in the dry, wet, and dry-after-wet states are shown in Figure 10, and the Segal crystallinities of all the samples in these three states are listed in Table 3. The Segal method is useful for comparing the relative differences between the CrIs of samples[43] irrespective of the fact that, in some cases, it is not a reliable method to estimate absolute CrI and amorphous and crystalline contributions.[44,45] Although not reported here, a cursory glance on the diffractograms in Figure 10 indicated that the (200) peak position, in most cases, was shifted to a higher value of 2θ in the wet-state XRDs. This shift has been previously reported by the authors.[16] As mentioned above, clearly, ball-milling reduces the CrI of the control MCC sample, and over a period of 120 min, the material becomes completely amorphous (Figure 2a, Table 3).[25] The CrI of the 120 min ball-milled sample (23.7%, Table 3), which is an entirely amorphous material, is not zero due to the limitation of the Segal method and for the same reason, the CrIs (Table 3) of the long duration milled samples are not low enough. This occurrence is a known limitation of the Segal method which gives higher CrIs for the low crystalline materials.[25,43]

https://doi.org/10.1021/acs.biomac.0c01389
Biomacromolecules 2021, 22, 1357−1373

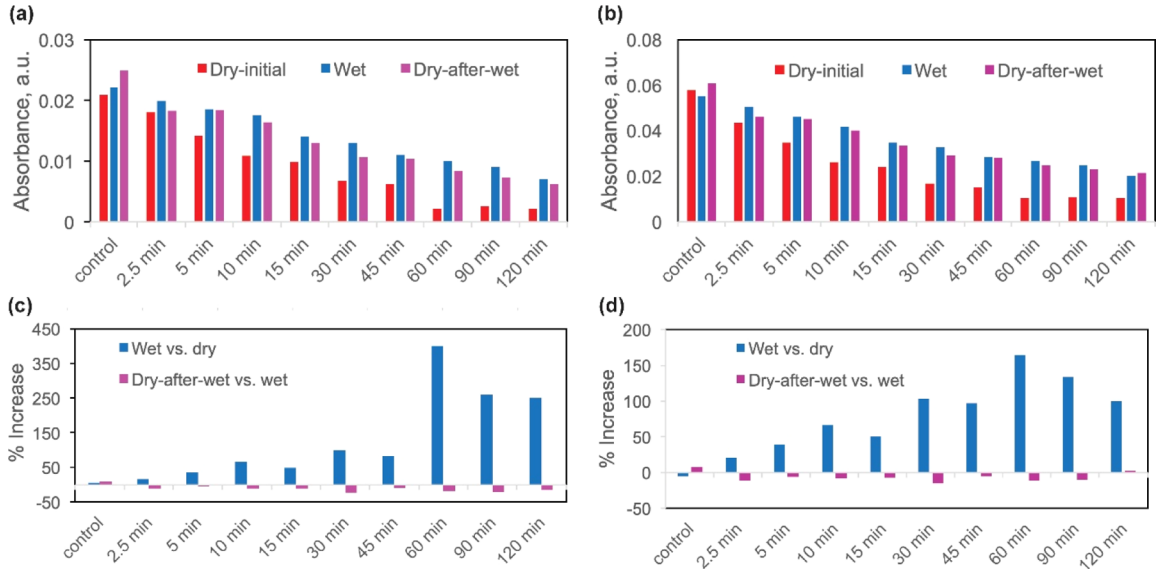

Figure 9. IR band absorbances in the three states of aggregation, (a) 1430 and (b) 1315 cm^{-1} in 1020 cm^{-1} normalized spectra; (c,d), % increases of band absorbance ratios when the ratios are compared between "wet and dry" and "dry-after-wet and wet" states—(c) I_{1430}/I_{1020} and (d) I_{1315}/I_{1020}.

Table 2. % Change[a] in IR Band Intensity Ratios

	wet vs dry		dry-after-wet vs wet		initial dry vs dry-after-wet	
samples	(I_{1429}/I_{1020})	(I_{1315}/I_{1020})	(I_{1429}/I_{1020})	(I_{1315}/I_{1020})	(I_{1429}/I_{1020})	(I_{1315}/I_{1020})
control	5.13	−5.56	9.76	7.84	−16.17	−5.03
2.5 min	14.71	20.73	−10.26	−11.11	−1.47	−5.48
5 min	37.04	39.39	−5.41	−6.52	−22.45	−22.85
10 min	66.67	66.00	−11.43	−8.43	−33.07	−35.00
15 min	47.37	50.00	−10.71	−7.25	−24.16	−28.27
30 min	100.00	103.13	−23.08	−15.38	−36.35	−43.02
45 min	83.33	96.55	−9.09	−5.26	−40.62	−46.85
60 min	400.00	165.00	−20.00	−11.32	−75.40	−58.13
90 min	260.00	133.33	−22.22	−10.20	−64.76	−52.91
120 min	250.00	100.00	−14.29	2.50	−67.17	−51.95

[a]Positive change means increase while negative change means decline in the ratio.

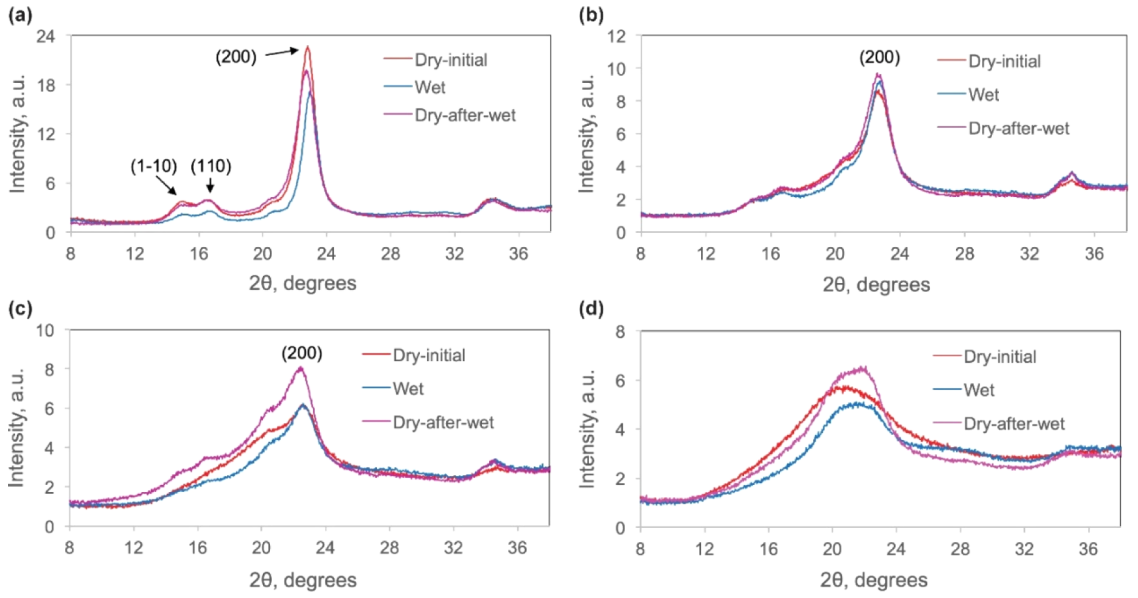

Figure 10. XRDs of selected samples in the three states of aggregation; (a) control and (b) 15, (c) 45, and (d) 120 min ball-milled samples.

https://doi.org/10.1021/acs.biomac.0c01389
Biomacromolecules 2021, 22, 1357−1373

Table 3. Segal Crystallinities and CrI Changes

	CrI, %			ΔCrI, %	
sample	dry, initial	wet	dry-after-wet	wet vs dry	dry-after-wet vs wet
control	89.7	91.5	89.7	2.0	−2.0
2.5 min	84.7	87.9	84.2	3.8	−4.2
5 min	79.0	83.3	78.7	5.4	−5.5
10 min	77.1	85	80.6	10.2	−5.2
15 min	67.8	76.6	71.6	13.0	−6.5
30 min	46.8	60.5	55.2	29.3	−8.8
45 min	45.1	58.8	54.5	30.4	−7.3
60 min	24.5	48.9	48.5	99.6	−0.8
90 min	25.9	44.2	44.4	70.7	0.5
120 min	23.7	42.3	40.9	78.5	−3.3

Nevertheless, the 120 min milled sample diffractogram in Figure 10d shows no peak at $2\theta \sim 22°$ and resembled other reported XRDs of amorphous celluloses.[40,43−48] Table 3 also lists CrIs of the samples in wet and dry-after-wet states. Moreover, in addition to changes in the CrIs (ΔCrIs, eqs 8 and 9), changes in the XRD peak profiles due to wetting and drying-after-wetting can be examined, as shown in Figure 10. Such information is important and, when appropriate, will be considered.

$$\Delta \mathrm{CrI}_{(\text{wet vs dry})} = (\mathrm{CrI}_{\text{wet}} - \mathrm{CrI}_{\text{dry}}) \times 100/\mathrm{CrI}_{\text{dry}} \quad (8)$$

$$\Delta \mathrm{CrI}_{(\text{dry-after-wet vs wet})} = (\mathrm{CrI}_{\text{dry-after-wet}} - \mathrm{CrI}_{\text{wet}}) \times 100/\mathrm{CrI}_{\text{wet}} \quad (9)$$

Compared to the dry state, wet-state CrIs were higher for all ball-milled MCCs (Table 3, Figures 10 and 11), and for the

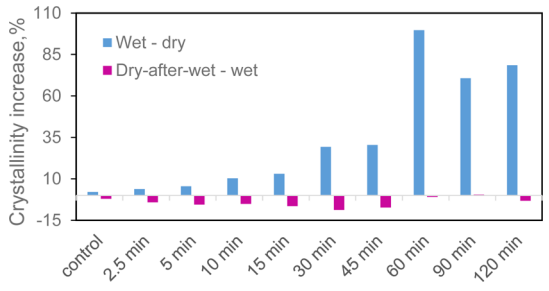

Figure 11. Change in Segal CrIs of ball-milled samples upon wetting and drying-after-wetting.

control sample, a small increase (2%, Table 3) was noted although it was within the experimental error range (<2%). In general, a higher increase in CrI was observed for the samples that were ball-milled for longer duration (Table 3), and the 60 min ball-milled sample showed the highest increase (100%) in CrI upon wetting. Moreover, there were significant changes in the XRD profiles of the samples (e.g., Figure 10c), suggesting that contributions from newly formed structures were present in many regions of the diffractogram. For instance, in the case of the 45 min ball-milled sample which, upon wetting, showed CrI increase of 30% (Table 3), the diffraction profile changed in most of the 14−22° 2θ range (Figure 10c). Compared to the dry state-diffractogram, in the wet state, the contribution declined in most sub-(200) peak position region (Figure 10c). The reason for the accidental matching of the intensity at 22.3° 2θ seems to be that the contributions of the initially present structures in the dry state (these would be decaying wing contributions at ~22° 2θ) were replaced by new contributions from the organized structures. In the wet state, the largest CrI change (99.6%, Table 3, Figure 11) was seen for the 60 min ball-milled sample. As reported above, this was also the case in IR where both the intensity ratios were enhanced by greater than 100% (Table 2, Figure 9). However, in Raman spectroscopy, due to the lack of a contribution at 380 cm^{-1} (zero peak intensity) in the spectrum of the 60 min ball-milled sample, the increase could not be calculated. Nevertheless, the 30 min ball-milling caused the I_{380}/I_{1096} ratio to increase by 441% (Table 1, Figure 4).

The effect of the moisture content on the XRDs of many cellulose materials has been previously reported.[14,16,35,49,50] Based on the authors' investigation of this topic,[16] the following was concluded—"changes in crystallinity, crystallite size, and peak position are likely to be associated with the alterations in the organization of cellulose and other sample components because the sample composition remains same." Other sample components were mentioned because in that work two classes of materials—those that contained mostly cellulose (e.g., tunicin, Avicel PH-101, and cotton MCC) and those that contained additional components (e.g., bleached kraft pulp and wood), were analyzed. Considering that in the present situation, the samples are almost entirely made up of cellulose, and it is fair to conclude that wetting caused alterations in the organization of cellulose, which impacted the XRDs of the investigated ball-milled samples.

Next, as was the case above in Raman and IR analyses, the effect of drying-after-wetting was examined (Table 3, Figure 11). Except in the 60 and 90 min ball-milled cases, where the changes were within the experimental error range (<3%), wet-state CrIs declined upon drying in all other cases, although the changes were small (<10%, Table 3, Figure 11). A maximum decline of 8.8% was noted for the 30 min ball-milled sample. This decline suggested that most of the organizational change in cellulose initiated by wetting was irreversible, an observation made above based on Raman and IR analyses. Nonetheless, some portion of the structure reverted to what was present in the initial dry state. Therefore, this XRD result further supported the conclusions drawn from Raman and IR studies that such alterable cellulose structures were non-crystalline and can contribute, in XRD, in the same regions as crystalline cellulose.

Accessibility to Water. Water accessibility of all of the samples was measured by the previously described Raman method that uses the intensity increase at 1380 cm^{-1},[5,24] a cellulose band, when all accessible CH_2OH groups in a sample are fully exchanged to CH_2OD (in short, OH-to-OD exchange). As described in the Materials and Methods section, the exchange was carried out by putting the samples in pure D_2O. This D_2O exchange was carried out for two sets of samples, initial dry and dry-after-wet (Table S3 and Figure 12). In all cases, compared to the dry state, the increment for the dry-after-wet state sample was lower and indicated that upon wetting the structural change was such that a portion became D_2O (and therefore, water) inaccessible. Based on the results obtained earlier, it is clear that wetting caused the structural transformation in cellulose but water accessibility information is likely to help further define this structural change.

Examples of 1380 cm^{-1} band intensity increases are shown in Figure 12a,b, respectively, for control and 60 min ball-milled samples that were OH-to-OD exchanged. The 1380 cm^{-1}

https://doi.org/10.1021/acs.biomac.0c01389
Biomacromolecules 2021, 22, 1357−1373

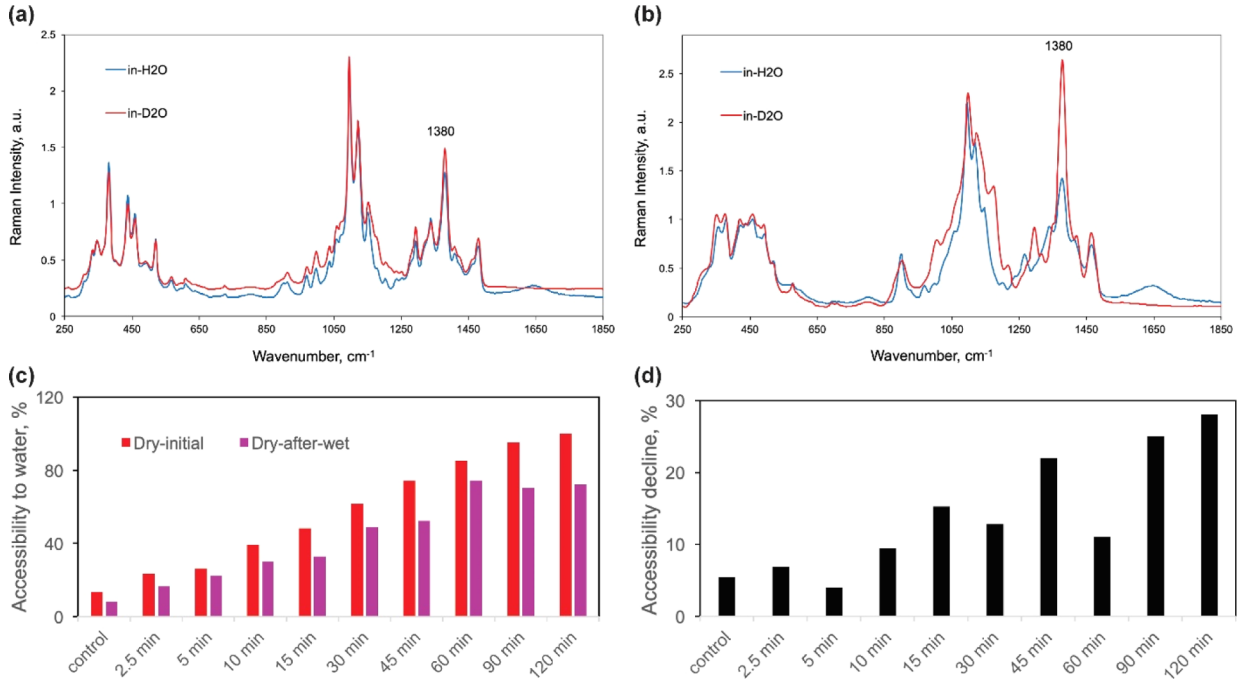

Figure 12. 1380 cm^{-1} band intensity increase in 1096 cm^{-1} normalized Raman spectra: (a) control, (b) 60 min ball-milled sample, (c) accessibility to water of dry and dry-after-wet samples, and (d) decline in water accessibility upon air drying at 25 °C.

peak-based percent intensity increase data for all the samples are summarized in Table S3. Such Raman experiments were repeated for the dry-after-wet samples, and surprisingly, lower % band intensity increases were obtained (Figure S3, Table S3). The accessibilities to water were calculated based on eq 1 in the Materials and Methods section.

Accessibility to water and its decline are reported in Table S3. The accessibility data are plotted in Figure 12c, and the decline in water accessibility is shown in Figure 12d. The highest decline (28%, Table S3) was observed for the 120 min milled sample. From these results, it is clear that post wetting, the modified cellulose structures had reduced-accessibility to D_2O (or water), further supporting the conclusion that the water-induced changes in the cellulose structure were partly irreversible.

Crystallinity differences between dry and dry-after-wet states further support these observations (Table 2) because higher crystallinity of the samples in dry-after-wet states will restrict water diffusion into the samples. Irrespective of not knowing the nature of the newly formed irreversible structure, crystalline or non-crystalline, its one distinguishing feature is that water cannot get in. One possibility is that such a structure is paracrystalline in nature because it has been reported that in such a phase, water cannot access the interior of the structure.[3]

Cellulose II Formation. There are four types of polymorphs of cellulose—cellulose I, cellulose II, cellulose III, and cellulose IV.[51] The first two forms are the most common and hence, of great interest. The I and II polymorphs differ not only with respect to their chain conformations and H-bonding but also in the fact that cellulose II has an anti-parallel structure. Compared to cellulose I, cellulose II has several enhanced properties such as dimensional stability, dyeability, reactivity, and luster.[52] Cellulose I is found in two sub-polymorphic forms called Iα and Iβ which are composed of different unit cells and therefore belong to different crystal space groups.[53] However, the chain conformations are identical between cellulose Iα and Iβ. Cotton MCC used in this study is classified as Iβ. Although both cellulose Iβ and cellulose II fall into the same monoclinic crystal space group $P2_1$, their unit cells are different.[44,51]

In Raman spectroscopy, cellulose II can be detected by the presence of a Raman vibrational mode at 577 cm^{-1} (Figure S1), a Raman frequency where amorphous and crystalline I forms of cellulose do not contribute.[37] Using eq 3, this band was used to quantify cellulose II amount in the samples.[27] It is well documented that amorphous cellulose when regenerated in water at room temperature gets converted to cellulose II.[38,42,46] In our study, cellulose II formation was detected only in those samples that were ball-milled for 15 min or longer (Figure 13). The Raman spectra are shown in Figure S4. After

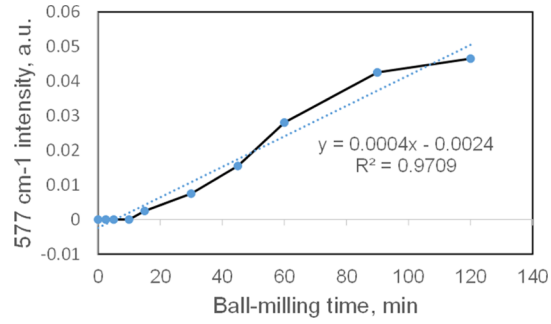

Figure 13. Correlation between Raman intensity of cellulose II 577 cm^{-1} band (in the wet state) and duration of ball milling.

15 min of ball-milling, the amount of cellulose II gradually increased linearly (R^2 = 0.97). The increase seems to be directly related to the amount of amorphous cellulose present in the ball-milled samples. When the samples were air dried at 25 °C, the wetting-generated amount of cellulose II did not diminish. Because the degree of polymerization (DP) of cellulose decreases only moderately with duration of ball-

https://doi.org/10.1021/acs.biomac.0c01389
Biomacromolecules 2021, 22, 1357−1373

milling,[25,39,54] it is unlikely that formation of cellulose II is related to cellulose DP. Another point to note is that compared to XRD, Raman spectroscopy seems to be more sensitive in detecting low levels of cellulose II because its reflections at 2θ = 20.1 and 12.3° were hardly detected in the diffractograms of the wet and dry-after-wet samples (e.g., Figure 10c,d).

Based on information from XRD, for the control sample, cellulose I amount (89.7%) was used. For all other samples, Raman information (Figures 4 and 13) was used to calculate the amounts of cellulose I (included cellulose I-like phase) and cellulose II polymorphs (Table 4). This table also lists the amount of amorphous cellulose which was simply calculated after subtracting the amounts of the two polymorphs from the total amount of the sample.

Table 4. Sample Composition (Cellulose I and Cellulose I-like; Amorphous[a]; Cellulose II)

control	89.7; 10.3; 0	92.3; 7.7; 0	75.7; 24.5; 0
2.5 min BM	66.4; 33.6; 0	78.6; 21.4; 0	60.2; 39.8; 0
5 min BM	48.2; 51.8; 0	74.1; 25.9; 0	54.8; 45.2; 0
10 min BM	35.9; 64.1; 0	59.9; 40; 0	50.3; 49.7; 0
15 min BM	38.5; 61.5; 0	61.7; 36.8; 1.5	53.8; 44.7; 1.5
30 min BM	7.3; 92.7; 0	39.5; 57; 3.5	23.2; 73.3; 3.5
45 min BM	0; 100; 0	35.7; 57.8; 6.5	27.9; 65.6; 6.5
60 min BM	0; 100; 0	26.4; 62.6; 11	18.8; 70.2; 11
90 min BM	0; 100; 0	24.1; 58.9; 17	16.1; 66.9; 17
120 min BM	0; 100; 0	18.5; 63.5; 18	13.8; 68.2; 18

[a]Amount of amorphous cellulose was calculated by subtracting cellulose I plus cellulose II amount from the total sample mass.

The table indicated that in the dry state, the amount of cellulose I declines continuously as a function of duration of ball milling. However, in the wet states, the amount of cellulose I (includes cellulose I-like) is higher compared to the dry and dry-after-wet states (Table 4). In Table 4, cellulose II is not present in any of the sample dry states and was first detected, in low amount, in the case of wet 15 min BM sample. However, in the wet samples, the amount of this polymorph continues to increase with the period of ball milling. Moreover, for a given sample, the cellulose II amounts were similar in the wet and dry-after-wet states. The maximum amount (18%, Table 4) of cellulose II existed in the 120 min BM sample.

PROPOSED SCHEME

Based on the findings of this investigation, the following scheme of transformations of the ball-milled cellulose, caused by water-induced changes and subsequent drying at 25 °C, is proposed. The scheme includes an initial decrystallization/amorphization step, which converts crystalline cellulose I to amorphous/disordered cellulose (Scheme 1), *X*. The amorphous cellulose amount *X* produced increases with the duration of the ball-milling. Upon wetting, this phase is transformed by water-induced reorganization to two cellulose I-like structures—reversible and irreversible (total amount X1, Scheme 1), along with cellulose II (Scheme 1, X2). The latter was detected only in 15 min or longer duration ball-milled samples. Upon air drying from the wet state, the reversible portion of the cellulose I structures reverts back to the original amorphous/disordered form (X3), whereas the irreversible form (X1−X3) does not undergo any further changes and retains the cellulose I-like phase. Additionally, upon drying, the amount of cellulose II formed by wetting does not change. Scheme 1 when applied to the 120 min sample relates most directly to the XRD patterns in Figure 10d, Raman spectra in Figures 3d, 5d, and 6d, and IR spectra in Figures 7d and 8d where the data for dry-initial, wet, and dry-after-wet states are shown.

Scheme 1. Structural Changes in Crystalline Cellulose I Upon Ball-Milling, Wetting, and Drying-after-Wetting at 25 °C; the Xs are Used to Designate the Various Forms Produced and Their Amounts in Different States

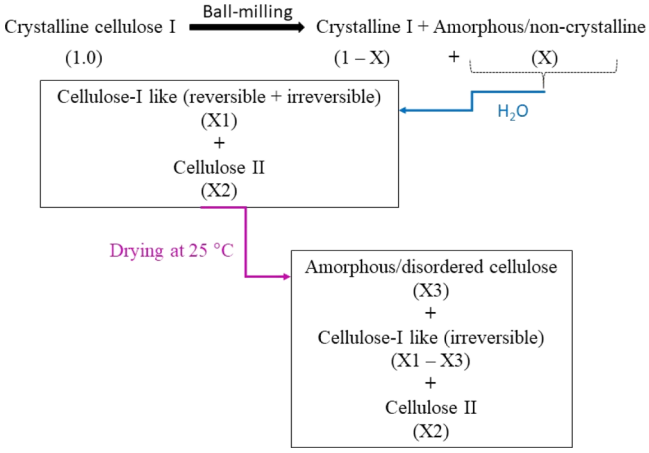

In Scheme 1, Xs are used to simplify the understanding of the various structural changes in cellulose. Quantitation of the phases can be carried out assuming cellulose I-like phase as cellulose I and using Raman spectroscopy to quantitate cellulose I and cellulose II (eqs 2 and 3).[27] Once these forms were quantified, the amount of amorphous cellulose was calculated by simply subtracting the total amount of cellulose I and cellulose II from the total mass of the sample (Table 4).

IMPLICATIONS

There are manifold implications of these findings. First, they have important consequences for the estimation of cellulose crystallinity using various methods (e.g., XRD, NMR, Raman, and IR). As described above, when such non-crystalline structures are present, the intensity of the peak(s) used in CrI estimation represents the sum of contributions of crystalline and non-crystalline states, and therefore, the estimated crystallinity is not accurate. The measured crystallinity depends upon the amount of aligned/organized cellulose that is present in a cellulose sample. In the presence of the latter, estimated CrI would be higher in XRD, NMR, and IR, and in 380-Raman, the change will depend upon which of the two peaks (1096 and 380 cm^{-1}), involved in the CrI determination, increases more. Recently, 380-Raman CrIs of CNCs when analyzed in the wet state were found to be lower. On the contrary, NMR estimation produced higher values.[23] In another measurement of crystallinity where two different NMR methods were used to estimate the CrIs of the ball-milled cotton,[17] it was reported that for the 45- and 120 min milled samples, the data diverged significantly, depending upon the method used. This is likely due to the fact that once water swollen, which is normally carried out in NMR measurements, the resultant structural changes contributed differently in the two methods. As indicated by the present investigation, such changes are much more significant at longer duration of ball milling (e.g., Figure 9).

https://doi.org/10.1021/acs.biomac.0c01389
Biomacromolecules 2021, 22, 1357−1373

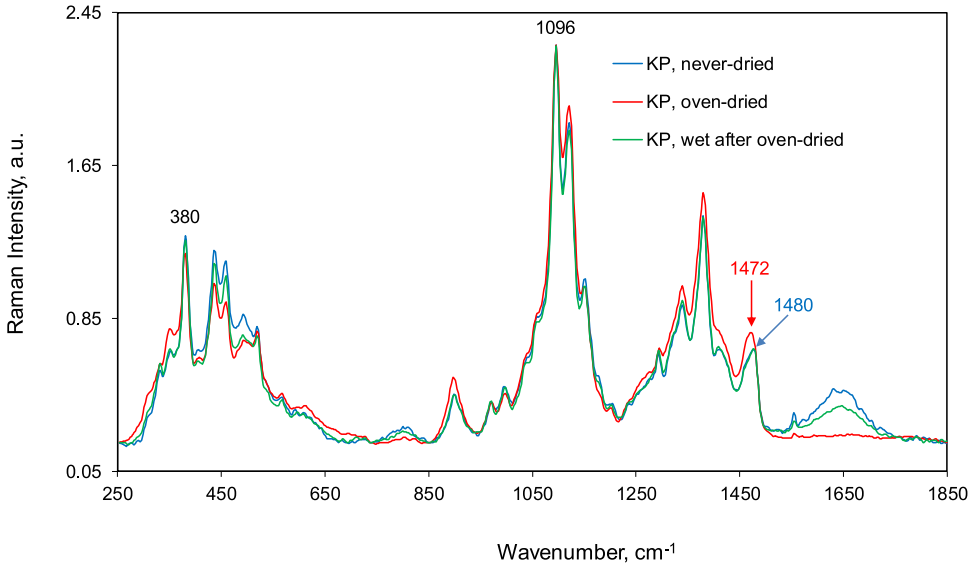

Figure 14. Raman spectra of bleached kraft pulp in never-dried, oven-dried, and wet after oven-dried states. Along with other peaks, CH_2 bending mode positions is annotated for never dried and oven-dried states.

Next, in materials that are not composed of highly crystalline cellulose, the effect of the increased moisture content on cellulose XRD (CrI and other diffraction-derived parameters) can now be simply explained by the idea that water causes reorganization of non-crystalline cellulose, thereby increasing the crystallinity and impacting other diffraction-derived parameters.[4,15,16] This explanation is contrary to the traditional view, based on assumptions, where moisture-induced dimensional changes in the cellulose crystals are considered to have been caused by the stresses of the environment,[4,55] including matrix substances (e.g., hemicellulose and lignin), if present. This view would only be correct if cellulose was 100% crystalline and showed a moisture-induced effect. Moreover, the latest research[4−6] is showing that in most of the wood-derived materials, cellulose exists either in semicrystalline, for example, wood pulp, or in the non-crystalline form, for example, wood cell wall, respectively. Furthermore, evidence from the recent research[56−59] has shown that xylan chains can be considered as integral parts of the microfibril structure, and therefore, their organization can also impact the XRD parameters.

Such changes in the interpretations of cellulose crystallinity have other implications. For instance, the phenomenon of co-crystallization becomes questionable.[9,13] Because not only no evidence exists for this phenomenon, but the increase in CrI reported in these investigations can simply be explained by the fact that in these materials, cellulose has become more crystalline.[6] For instance, compared to untreated wood, hydrothermally treated wood was found to have a higher cellulose CrI because the cellulose in untreated wood was not crystalline.[5,6]

Another area where this finding has relevance is the biosynthesis of cellulose. It was shown in 2016 that the native state of wood cell wall cellulose is non-crystalline although it produced cellulose I-like features in Raman, IR, and XRD analyses.[5] The conditions of biosynthesis under which cellulose aggregates and the conditions used in this study, water at 25 °C, both are identical, and therefore, the latter may serve as a model system to examine the biosynthesis of cellulose and to understand the structure of cellulose microfibril. There are many more implications, but they cannot be fully developed here due to the nature of this paper. In any case, the findings of this investigation will be beneficial to many groups including biologists, biochemists, chemists, and material scientists.

Real-World Applications. Few cellulose materials were analyzed to see whether the results of this study apply to them. One of the samples selected was bleached kraft pulp which has been studied previously in the authors laboratory[5] and by other researchers.[60] This pulp was analyzed in three states, never-dried, oven-dried and wet after oven-dried. The spectra are shown in Figure 14. Upon close spectral examination, among other changes, it was observed that due to oven-drying, 380 cm^{-1} peak declined in intensity, region 900−1250 cm^{-1} had lower spectral resolution, and the peak at 1480 cm^{-1} had shifted to 1472 cm^{-1}. However, most of these changes were reversible because upon wetting, the dried pulp spectrum reverted to a spectrum that was very similar to the original spectrum obtained in the never-dried state (Figure 14). This observation indicated that the non-crystalline portion of cellulose in pulp fibers was responsible for such changes because the crystalline fraction cannot undergo reversible changes. The interpretation of the observed Raman changes in terms of the findings in this study was that, in the never-dried state, the non-crystalline cellulose structure in pulp fibers contributed at the same spectral positions as the crystalline cellulose. However, upon oven-drying, such a structure became disordered due to it being non-crystalline. Subsequently though, upon rewetting, it reorganized to its original form and once again contributed like crystalline cellulose.

CONCLUSIONS

Supramolecular structures of cellulose and their modification by water were investigated in this study using Raman, IR, and XRD analyses. Studies of control and ball-milled cotton MCC samples in dry, wet, and dry-after-wet states indicated that upon wetting, new structures are formed that contributed, in Raman, IR, and XRD in the same regions where crystalline cellulose I contributions are detected. Such structures were of two types, those that post wetting, when air dried at 25 °C, retained their newly formed phase (irreversible) and those

https://doi.org/10.1021/acs.biomac.0c01389
Biomacromolecules 2021, 22, 1357−1373

that, upon air drying at 25 °C, reverted to their original dry state form (reversible). Between the two newly formed phases, which were both generated due to water-induced changes, the irreversible phase was dominant. Although this form can be classified as crystalline cellulose I, because regeneration of cellulose I from completely amorphous cellulose at 25 °C is not known to occur, further work is needed to accurately categorize it. The reversible phase, which was present in lower amount, however, was non-crystalline. These findings have important implications for several areas, for example, estimation of cellulose crystallinity, moisture-induced changes to crystallinity, and the phenomenon of cocrystallization.

■ ASSOCIATED CONTENT

Supporting Information

The Supporting Information is available free of charge at https://pubs.acs.org/doi/10.1021/acs.biomac.0c01389.

Intensity ratios for selected Raman bands and intensities of selected IR bands; 1380 cm^{-1} band intensity increase and water accessibility data; Raman spectrum of cellulose II; IR OH stretch region for 45- and 120 min ball-milled samples in dry and dry-after-wet states; bar chart of % 1380 cm^{-1} band intensity increases for the samples; and Raman spectra showing cellulose II peak at 577 cm^{-1} (PDF)

■ AUTHOR INFORMATION

Corresponding Author

Umesh P. Agarwal − *Fiber and Chemical Sciences Research, USDA FS, Forest Products Laboratory, Madison, Wisconsin 53726-2398, United States;* orcid.org/0000-0002-5509-1961; Phone: (608) 231-9441; Email: umesh.p.agarwal@usda.gov

Authors

Sally A. Ralph − *Fiber and Chemical Sciences Research, USDA FS, Forest Products Laboratory, Madison, Wisconsin 53726-2398, United States*

Carlos Baez − *Fiber and Chemical Sciences Research, USDA FS, Forest Products Laboratory, Madison, Wisconsin 53726-2398, United States*

Richard S. Reiner − *Fiber and Chemical Sciences Research, USDA FS, Forest Products Laboratory, Madison, Wisconsin 53726-2398, United States*

Complete contact information is available at: https://pubs.acs.org/10.1021/acs.biomac.0c01389

Notes

The authors declare no competing financial interest.

■ ACKNOWLEDGMENTS

The authors thank Tom Kuster (retired) of Analytical Chemistry and Microscopy Laboratory for his help in obtaining SEMs. The authors gratefully acknowledge the use of X-ray facilities and instrumentation supported by NSF through the University of Wisconsin Materials Research Science and Engineering Center (DMR-1121288).

■ REFERENCES

(1) Atalla, R. H. The Structures of Cellulose. In *Materials Interactions Relevant to the Pulp, Paper, and Wood Industries: Proceedings, Materials Research Society Symposium*, 1990 April 18−20; Caulfield, D. F., Passaretti, J. D., Sobczynski, S. F., Eds.; Materials Research Society: San Francisco, CA Pittsburgh, PA, 1990; Vol. *197*, pp 89−98.

(2) Klemm, D.; Heublein, B.; Fink, H.-P.; Bohn, A. Cellulose: Fascinating biopolymer and sustainable raw material. *Angew. Chem., Int. Ed.* **2005**, *44*, 3358−3393.

(3) Larsson, P. T.; Wickholm, K.; Iversen, T. A CP/MAS ^{13}C NMR investigation of molecular ordering in celluloses. *Carbohydr. Res.* **1997**, *302*, 19−25.

(4) Toba, K.; Yamamoto, H.; Yoshida, M. Crystallization of cellulose microfibrils in wood cell wall by repeated dry-and-wet treatment, using X-ray diffraction technique. *Cellulose* **2013**, *20*, 633−643.

(5) Agarwal, U. P.; Ralph, S. A.; Reiner, R. S.; Baez, C. Probing crystallinity of never-dried wood cellulose with Raman spectroscopy. *Cellulose* **2016**, *23*, 125−144.

(6) Agarwal, U. P.; Ralph, S. A.; Reiner, R. S.; Baez, C. New cellulose crystallinity estimation method that differentiates between organized and crystalline phases. *Carbohydr. Polym.* **2018**, *190*, 262−270.

(7) Penttilä, P. A.; Altgen, M.; Carl, N.; van der Linden, P.; Morfin, I.; Osterberg, M.; Schweins, R.; Rautkari, L. Moisture-related changes in the nanostructure of woods studied with X-ray and neutron scattering. *Cellulose* **2020**, *27*, 71−87.

(8) Chen, L.; Wang, Q.; Hirth, K.; Baez, C.; Agarwal, U. P.; Zhu, J. Y. Tailoring the yield and characteristics of wood cellulose nanocrystals (CNC) using concentrated acid hydrolysis. *Cellulose* **2015**, *22*, 1753−1762.

(9) Newman, R. H. Carbon-13 NMR evidence for cocrystallization of cellulose as a mechanism for hornification of bleached kraft pulp. *Cellulose* **2004**, *11*, 45−52.

(10) Nazhad, M. M.; Paszner, L. Fundamentals of strength loss in recycled paper. *Tappi J.* **1994**, *77*, 171−179.

(11) Leboucher, J.; Bazin, P.; Goux, D.; El Siblani, H.; Travert, A.; Barbulée, A.; Bréard, J.; Duchemin, B. High-yield cellulose hydrolysis by HCl vapor: co-crystallization, deuterium accessibility and high-temperature thermal stability. *Cellulose* **2020**, *27*, 3085−3105.

(12) Kontturi, E.; Meriluoto, A.; Penttilä, P. A.; Baccile, N.; Malho, J.-M.; Potthast, A.; Rosenau, T.; Ruokolainen, J.; Serimaa, R.; Laine, J.; Sixta, H. Degradation and crystallization of cellulose in hydrogen chloride vapor for high-yield isolation of cellulose nanocrystals. *Angew. Chem., Int. Ed.* **2016**, *55*, 14455−14458.

(13) Kuribayashi, T.; Ogawa, Y.; Rochas, C.; Matsumoto, Y.; Heux, L.; Nishiyama, Y. Hydrothermal transformation of wood cellulose crystals into pseudo-orthorhombic structure by cocrystallization. *ACS Macro Lett.* **2016**, *5*, 730−734.

(14) Hill, S. J.; Kirby, N. M.; Mudie, S. T.; Hawley, A. M.; Ingham, B.; Franich, R. A.; Newman, R. H. Effect of drying and rewetting of wood on cellulose molecular packing molecular packing. *Holzforschung* **2010**, *64*, 421−427.

(15) Abe, K.; Yamamoto, H. Change in mechanical interaction between cellulose microfibril and matrix substance in wood cell wall induced by hygrothermal treatment. *J. Wood Sci.* **2006**, *52*, 107−110.

(16) Agarwal, U. P.; Ralph, S. A.; Baez, C.; Reiner, R. S.; Verrill, S. P. Effect of sample moisture content on XRD-estimated cellulose crystallinity index and crystallite size. *Cellulose* **2017**, *24*, 1971−1984.

(17) Ling, Z.; Wang, T.; Makarem, M.; Santiago Cintrón, M.; Cheng, H. N.; Kang, X.; Bacher, M.; Potthast, A.; Rosenau, T.; King, H.; Delhom, C. D.; Nam, S.; Vincent Edwards, J.; Kim, S. H.; Xu, F.; French, A. D. Effects of ball milling on the structure of cotton cellulose. *Cellulose* **2019**, *26*, 305−328.

(18) Su, Y.; Burger, C.; Ma, H.; Chu, B.; Hsiao, B. S. Exploring the nature of cellulose microfibrils. *Biomacromolecules* **2015**, *16*, 1201−1209.

(19) Li, Q.; Renneckar, S. Supramolecular structure characterization of molecularly thin cellulose I nanoparticles. *Biomacromolecules* **2011**, *12*, 650−659.

(20) Li, Z.; Sathitsuksanoh, N.; Zhang, W.; Goodell, B.; Renneckar, S. Towards an understanding of cellulose microfibril dimensions from TEMPO-oxidized pulp fiber. In *Nanocelluloses: Their Preparation, Properties, and Applications*; Agarwal, U. P.; Atalla, R. H.; Isogai, A.,

Eds.; ACS Symposium Series #1251; American Chemical Society: Washington DC, 2017; Chapter 3.
(21) Agarwal, U. P.; Reiner, R. R.; Ralph, S. A. Estimation of cellulose crystallinity of lignocelluloses using near-IR FT−Raman spectroscopy and comparison of the Raman and Segal-WAXS methods. *J. Agric. Food Chem.* **2013**, *61*, 103−113.
(22) Wormald, P.; Wickholm, K.; Larsson, P. T.; Iversen, T. Conversions between ordered and disordered cellulose: Effects of mechanical treatment followed by cyclic wetting and drying. *Cellulose* **1996**, *3*, 141−152.
(23) Agarwal, U. P.; Reiner, R. S.; Ralph, S. A.; Catchmark, J.; Chi, K.; Foster, E. J.; Hunt, C. G.; Baez, C.; Ibach, R. E.; Hirth, K. C. Characterization of the supramolecular structures of cellulose nanocrystals of different origins. *Cellulose* **2021**, *28*, 1369−1385.
(24) Lee, C. M.; Kafle, K.; Belias, D. W.; Park, Y. B.; Glick, R. E.; Haigler, C. H.; Kim, S. H. Comprehensive analysis of cellulose content, crystallinity, and lateral packing in Gossypium hirsutum and Gossypium barbadense cotton fibers using sum frequency generation, infrared and Raman spectroscopy, and X-ray diffraction. *Cellulose* **2015**, *22*, 971−989.
(25) Agarwal, U. P.; Reiner, R. S.; Ralph, S. A. Cellulose I crystallinity determination using FT−Raman spectroscopy: univariate and multivariate methods. *Cellulose* **2010**, *17*, 721−733.
(26) Foster, E. J.; Moon, R. J.; Agarwal, U. P.; Bortner, M. J.; Bras, J.; Camarero-Espinosa, S.; Chan, K. J.; Clift, M. J. D.; Cranston, E. D.; Eichhorn, S. J.; Fox, D. M.; Hamad, W. Y.; Heux, L.; Jean, B.; Korey, M.; Nieh, W.; Ong, K. J.; Reid, M. S.; Renneckar, S.; Roberts, R.; Shatkin, J. A.; Simonsen, J.; Stinson-Bagby, K.; Wanasekara, N.; Youngblood, J. Current characterization methods for cellulose nanomaterials. *Chem. Soc. Rev.* **2018**, *47*, 2609−2679.
(27) Agarwal, U. P. Raman spectroscopy in the analysis of cellulose nanomaterials. In *Nanocelluloses: Their Preparation, Properties, and Applications*; Agarwal, U. P.; Atalla, R. H.; Isogai, A., Eds.; ACS Symposium Series #1251; American Chemical Society: Washington DC, 2017; Chapter 4.
(28) Segal, L.; Creely, J. J.; Martin, A. E.; Conrad, C. M. An empirical method for estimating the degree of crystallinity of native cellulose using the x-ray diffractometer. *J. Text. Res.* **1959**, *29*, 786−794.
(29) Liang, C. Y.; Marchessault, R. H. Infrared spectra of crystalline polysaccharides. I. Hydrogen bonds in native celluloses. *J. Polym. Sci.* **1959**, *37*, 385−395.
(30) Schwanninger, M.; Rodrigues, J. C.; Pereira, H.; Hinterstoisser, B. Effects of short-time vibratory ball milling on the shape of FT-IR spectra of wood and cellulose. *Vib. Spectrosc.* **2004**, *36*, 23−40.
(31) Lindh, E. L.; Bergenstråhle-Wohlert, M.; Terenzi, C.; Salmén, L.; Furó, I. Non-exchanging hydroxyl groups on the surface of cellulose fibrils: the role of interaction with water. *Carbohydr. Res.* **2016**, *434*, 136−142.
(32) Abidi, N.; Cabrales, L.; Haigler, C. H. Changes in the cell wall and cellulose content of developing cotton fibers investigated by FTIR spectroscopy. *Carbohydr. Polym.* **2014**, *100*, 9−16.
(33) Nelson, M. L.; O'Connor, R. T. Relation of certain infrared bands to cellulose crystallinity and crystal lattice type. Part I. Spectra of lattice Types I, II, III and of amorphous cellulose. *J. Appl. Polym. Sci.* **1964**, *8*, 1311−1324.
(34) Nelson, M. L.; O'Connor, R. T. Relation of Certain Infrared Bands to Cellulose Crystallinity and Crystal Lattice Type. Part II. A new infrared ratio for estimation of crystallinity in celluloses I and II. *J. Appl. Polym. Sci.* **1964**, *8*, 1325−1341.
(35) Oh, S. Y.; Yoo, D. I.; Shin, Y.; Kim, H. C.; Kim, H. Y.; Chung, Y. S.; Park, W. H.; Youk, J. H. Crystalline structure analysis of cellulose treated with sodium hydroxide and carbon dioxide by means of X-ray diffraction and FTIR spectroscopy. *Carbohydr. Res.* **2005**, *340*, 2376−2391.
(36) Schenzel, K.; Fischer, S.; Brendler, E. New method for determining the degree of cellulose I CrI by means of FT Raman spectroscopy. *Cellulose* **2005**, *12*, 223−231.
(37) Agarwal, U. P. 1064 nm FT-Raman spectroscopy for investigations of plant cell walls and other biomass materials. *Front. Plant Sci.* **2014**, *5*, 490.
(38) Caulfield, D. F.; Steffes, R. A. Water-induced recrystallization of cellulose. *Tech. Assoc. Pulp Pap. Ind.* **1969**, *52*, 1361−1366.
(39) Howsmon, J. A.; Marchessault, R. H. The ball-milling of cellulose fibers and recrystallization effects. *J. Appl. Polym. Sci.* **1959**, *1*, 313−322.
(40) Wadehra, I. L.; Manley, R. S. J. Recrystallization of amorphous cellulose. *J. Appl. Polym. Sci.* **1965**, *9*, 2627−2630.
(41) Tyufekchiev, M.; Kolodziejczak, A.; Duan, P.; Foston, M.; Schmidt-Rohr, K.; Timko, M. T. Reaction engineering implications of cellulose crystallinity and water-promoted recrystallization. *Green Chem.* **2019**, *21*, 5541−5555.
(42) Atalla, R. H.; Nagel, S. C. Cellulose: Its regeneration in the native lattice. *Science* **1974**, *185*, 522−523.
(43) Park, S.; Baker, J. O.; Himmel, M. E.; Parilla, P. A.; Johnson, D. K. Cellulose crystallinity index: measurement techniques and their impact on interpreting cellulase performance. *Biotechnol. Biofuels* **2010**, *3*, 10.
(44) Nam, S.; French, A. D.; Condon, B. D.; Concha, M. Segal crystallinity index revisited by the simulation of X-raydiffraction patterns of cotton cellulose Iβ and cellulose II. *Carbohydr. Polym.* **2016**, *135*, 1−9.
(45) French, A. D.; Santiago Cintrón, M. Cellulose polymorphy, crystallite size, and the Segal crystallinity index. *Cellulose* **2013**, *20*, 583−588.
(46) Atalla, R. H.; Ellis, J. D.; Schroeder, L. R. Some effects of elevated temperatures on the structure of cellulose and its transformation. *J. Wood Chem. Technol.* **1984**, *4*, 465−482.
(47) Schroeder, L. R.; Gentile, V. M.; Atalla, R. H. Nondegradative preparation of amorphous cellulose. *J. Wood Chem. Technol.* **1986**, *6*, 1−14.
(48) Ciolacu, D.; Ciolacu, F.; Popa, V. I. Amorphous cellulose − structure and characterization. *Cellul. Chem. Technol.* **2011**, *45*, 13−21.
(49) Abe, K.; Yamamoto, H. Mechanical interaction between cellulose microfibril and matrix substance in wood cell wall determined by X-ray diffraction. *J. Wood Sci.* **2005**, *51*, 334−338.
(50) Bhuiyan, M. T. R.; Hirai, N.; Sobue, N. Changes of crystallinity in wood cellulose by heat treatment under dried and moist conditions. *J. Wood Sci.* **2000**, *46*, 431−436.
(51) Zugenmaier, P. *Crystalline Cellulose and Cellulose Derivatives*; Springer Verlag: Berlin, Germany, 2010; pp 101−174.
(52) Cook, J. G. *Handbook of Textile Fibres, Volume I. Natural Fibres*; Woodhead Publishing: Cambridge, United Kingdom, 1984.
(53) Atalla, R. H.; Vanderhart, D. L. Native cellulose: A composite of two distinct crystalline forms. *Science* **1984**, *223*, 283−285.
(54) Mattonai, M.; Pawcenis, D.; del Seppia, S.; Łojewska, J.; Ribechini, E. Effect of ball-milling on crystallinity index, degree of polymerization and thermal stability of cellulose. *Bioresour. Technol.* **2018**, *270*, 270−277.
(55) Sobue, N.; Shibata, Y.; Mizusawa, T. X-ray measurement of lattice strain of cellulose crystals during the shrinkage of wood in the longitudinal direction (in Japanese). *Mokuzai Gakkaishi* **1992**, *38*, 336−724.
(56) Jarvis, M. C. Structure of native cellulose microfibrils, the starting point for nanocellulose manufacture. *Philos. Trans. R. Soc., A* **2018**, *376*, 20170045.
(57) Simmons, T. J.; Mortimer, J. C.; Bernardinelli, O. D.; Poppler, A.-C.; Brown, S. P.; deAzevedo, E. R.; Dupree, R.; Dupree, P. Folding of xylan onto cellulose fibrils in plant cell walls revealed by solid state NMR. *Nat. Commun.* **2016**, *7*, 13902.
(58) Thomas, L. H.; Forsyth, V. T.; Martel, A.; Grillo, I.; Altaner, C. M.; Jarvis, M. C. Structure and spacing of cellulose microfibrils in woody cell walls of dicots. *Cellulose* **2014**, *21*, 3887−3895.
(59) Thomas, L. H.; Martel, A.; Grillo, I.; Jarvis, M. C. Hemicellulose binding and the spacing of cellulose microfibrils in spruce wood. *Cellulose* **2020**, *27*, 4249−4254.

https://doi.org/10.1021/acs.biomac.0c01389
Biomacromolecules 2021, 22, 1357−1373

(60) Kesari, K. K.; Leppänen, M.; Ceccherini, S.; Seitsonen, J.; Väisänen, S.; Altgen, M.; Johansson, L.-S.; Maloney, T.; Ruokolainen, J.; Vuorinen, T. Chemical characterization and ultrastructure study of pulp fibers. *Mater. Today Chem.* **2020**, *17*, 100224.

https://doi.org/10.1021/acs.biomac.0c01389
Biomacromolecules 2021, 22, 1357−1373